UT GSBS Dissertations and Theses (Open Access)          Graduate School of Biomedical Sciences

8-2013

# CONFORMATIONAL DYNAMICS OF K-RAS AND H-RAS PROTEINS: IS THERE FUNCTIONAL SPECIFICITY AT THE CATALYTIC DOMAIN?

NANDINI RAMBAHAL

Recommended Citation

CONFORMATIONAL DYNAMICS OF K-RAS AND H-RAS PROTEINS: IS THERE FUNCTIONAL

SPECIFICITY AT THE CATALYTIC DOMAIN?

by

Nandini Rambahal, B.S.

APPROVED:

_____

Alemayehu Gorfe, PhD
Supervisory Committee Chair


_____

Jeffrey Frost, PhD


_____

John Putkey, PhD


_____

James Briggs, PhD


_____

Lei Zheng, PhD


APPROVED:

_____

Dean, The University of Texas
Graduate School of Biomedical Sciences at Houston

CONFORMATIONAL DYNAMICS OF K-RAS AND H-RAS PROTEINS: IS THERE

FUNCTIONAL SPECIFICITY AT THE CATALYTIC DOMAIN?


A

THESIS


Presented to the Faculty

of

The University of Texas

Health Science Center at Houston

and

The University of Texas MD Anderson Cancer Center

Graduate School of Biomedical Sciences

in Partial Fulfillment

of the Requirements

for the Degree of

MASTER OF SCIENCE


by

Nandini Rambahal, B.S.

Houston, Texas

August 2013

## Acknowledgements

Firstly I would like to thank my mentor Dr. Alemayehu Gorfe for his support and guidance in completing this project. His superb mentorship, patience and persistence helped me to transition from a background in experimental biochemistry to computational biology and to achieve this milestone in my academic career.

I would like to acknowledge the support of my colleagues in the Gorfe group, Harrison, Hualin, Priyanka and Zhenlong. The comradeship and cooperation within this group and the eagerness to help and discuss new ideas has provided a wonderful environment for intellectual growth but even more so laughter and friendship.

Members of my supervisory and advisory committee, Dr. James Briggs, Dr. Jeffrey Frost, Dr. John Putkey, Dr. Lei Zheng and Dr. Vasanthi Jayaraman have each provided invaluable insight towards the completion of this work. Each member brought a unique perspective to my work and I am forever thankful for their contributions and willingness to evaluate my performance.

The support and love of my parents has been a beacon for me. Through their strength I have found mine. Being a middle child I am lucky to have the friendship of an older brother and younger sister, who assure me that I'm not completely weird. I have to acknowledge my babies, my two cats for giving me a reason to go home every night and through constantly sleeping on my laptop and chewing my papers, reminding me that I also need to sleep.

Lastly I would like to thank my husband, Zhenlong for his love, wisdom, guidance and patience and mostly his faith in my ability to complete this work.

CONFORMATIONAL DYNAMICS OF K-RAS AND H-RAS PROTEINS: IS THERE FUNCTIONAL

SPECIFICITY AT THE CATALYTIC DOMAIN?

Nandini Rambahal B.S.

Supervisory Professor: Alemayehu Gorfe, Ph.D

Ras proteins serve as crucial signaling modulators in cell proliferation through their ability to hydrolyze GTP and exist in a GTP "on" state and GTP "off" state. There are three different human Ras isoforms: H-ras, N-ras and K-ras (4A and 4B). Although their sequence identity is very high at the catalytic domain, these isoforms differ in their ability to activate different effectors and hence different signaling pathways. Much of the previous work on this topic has attributed this difference to the hyper variable region of Ras proteins, which contains most of the sequence variance among the isoforms and encodes specificity for differential distribution in the membrane. However, we hypothesize *that sequence variation on lobe II of Ras catalytic domain alters dynamics and leads to differential preference for different effectors or modulators.* In this work, we used all atom molecular dynamics to analyze the dynamics in the catalytic domain of H-ras and K-ras. We have also analyzed the dynamics of a transforming mutant of H-ras and K-ras and further studied the dynamics of an effector-selective mutant of H-ras. Collectively we have determined that wild type K-ras is more dynamic than H-ras and that the structure of the effector binding loop more closely resembles that of the T35S Raf-selective mutant, possibly giving us a new view and insight into the

mode of effector specificity. Furthermore we have determined that specific mutations at the same location perturb the conformational equilibrium differently in H-ras and K-ras and that an enhanced oncogenic potential may arise from different structural perturbations for each point mutation of a specific isoform.

# Table of Contents

**CHAPTER 1: INTRODUCTION**

**CHAPTER 2: OVERVIEW MOLECULAR DYNAMICS SIMULATIONS AND KEY TRAJECTORY**

**ANALYSIS TECHNIQUES**

**CHAPTER 3: METHODS**

**CHAPTER 4: RESULTS AND DISCUSSION RAS DYNAMICS**

# List of Illustrations

## CHAPTER 5

# List of Tables

# List of Abbreviations

α1, α2…………………………………………………....….Alpha helix 1, Alpha helix 2 etc

BLAST …………………………………………..…Basic Local Alignment Search Tool

β1, β2……………………………………….………....…Beta Sheet 1, beta sheet 2 etc

DCCM………………………………….…………….. Dynamic Cross Correlation Matrix

CRD……………………………………….………………….Cystine Rich Domain

GDP………………………………..……………………… Guanosine Diphosphate

GTP…………………………………………..…………. Guanosine Triphosphate

HVR……………………………………….……………Hypervariable Region

L1 L10…………………………………..………………...Loop 1, Loop 10 etc

MAPK…………………………………………..…… Mitogen-Activated Protein Kinase

MD………………………………………..………….. Molecular Dynamics

$Mg^{2+}$ …………………………………………………..….…………….Magnesium ion

PCA………………………………………………… Principal Component Analysis

PC ………………………………………………………..Principal Component

PDB……………………………………………...……………. Protein Data Bank

PI3K………………………………………………..……… Phosphoinositide 3-kinase

RBD…………………………………………….………..…Ras Binding Domain

RMSD………………………………………..…… Root Mean Square Deviation

RMSF……………………………………….…... Root Mean Square Fluctuation

VMD…………………………………………..………… Visual Molecular Dynamics

WT……………………………………….……………….……Wild Type

<center>**Chapter 1**</center>

<center>**Introduction**</center>

## 1.1 History of Ras and Biological Function

RAS genes were initially discovered in rodent viral oncogenes that were capable of inducing sarcomas in new-born rodents [1,2]. To date constitutively active Ras mutants have been implicated in about 30% of human cancers, and it has been the target of numerous biochemical and biological studies in the field of cancer research [3,4].

Ras proteins (Ras) belong to the Ras Superfamily of GTPases, which function as small (21kDa) molecular switches by cycling between an "ON" GTP-bound and "OFF" GDP-bound conformational states. While members of the Ras superfamily share similarity to heterotrimeric G protein $\alpha$ subunits in both their biochemistry and function, they are monomeric [5,6]. Ras proteins function as signaling modulators through cell surface receptors to activate various effector pathways that control cellular proliferation, differentiation, or cell death [6,7]. Ras associates with guanine nucleotides (GTP/GDP) with high affinity and possesses intrinsic GTPase activity. The slow GTPase activity of Ras is accelerated by binding to specific GTPase activating proteins (GAPs) [8] resulting in an inactive state of the protein since Ras·GDP has low affinity for effectors [9]. Ras activation is then achieved through the association of Ras·GDP with guanine nucleotide exchange factors (GEFs) which displace GDP for the more abundant GTP in the cell [10]. Activated Ras then interacts with several downstream effectors including the Raf kinase, phosphoinositide 3-kinase $\gamma$ (PI3K) and RalGDS in response to growth factor stimulation.

<center>1</center>
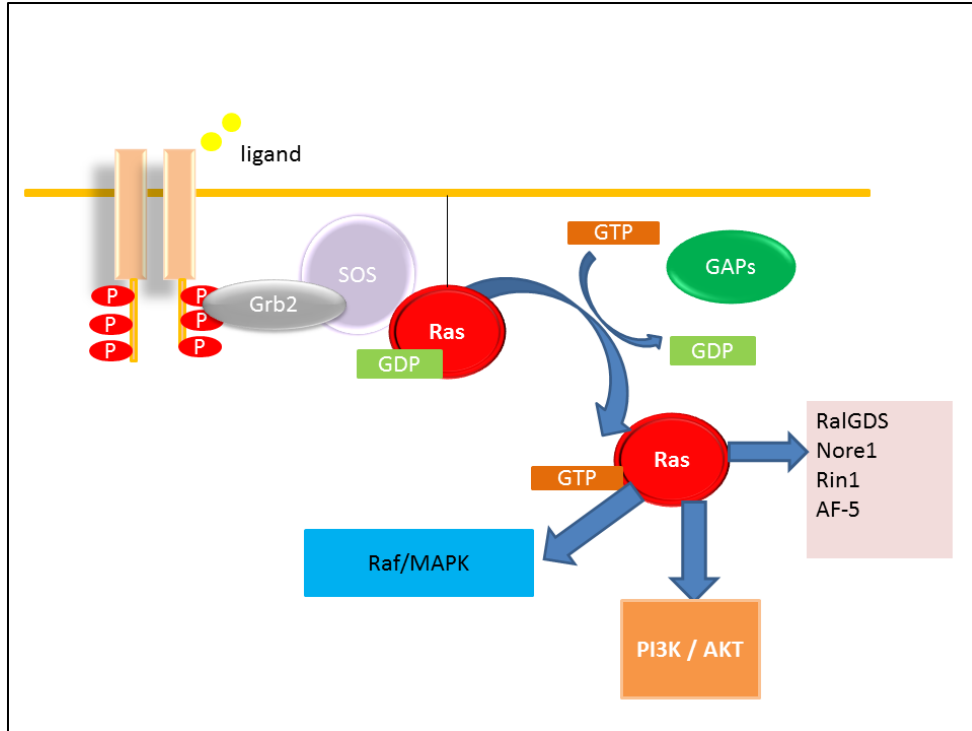
**Figure 1.1** Schematic of Ras signaling in the cell[1]

## 1.2 Ras Structure

Members of the Ras superfamily all possess a G-box or P-loop sequence, which is a signature of the purine nucleotide binding motif VAAAAGXXXXGK(S/T), where A is either leucine, isoleucine or valine, and X is any amino acid [11]. On Ras the P-loop consists of amino acids 10 to 17. Human Ras proteins consist of four highly homologous isoforms; H-ras, N-ras and K-ras (4A and 4B). The Ras protein structure can be divided into two lobes. Lobe I (residues 1-80) is 100 % conserved amongst the isoforms. In lobe II (residues 80-160) there is ~ 70-80% sequence identity between any pair of vertebrate RAS gene products [12]. Together lobes I and II comprise the catalytic domain. The hyper variable region (HVR) is composed of the remaining 25/26 amino acids and is highly variable except for the last 4 residues which are conserved amongst RAS and related genes. These last four residues form

---

[1] This image was created based on numerous reviews and illustrations of Ras signaling for the purpose of this thesis.

the CAAX motif, where A is any aliphatic amino acid X is any amino acid [12]. Ras proteins undergo differential post-translational modification at the C-terminus, which are crucial for membrane binding [13]. Mutations at the CAAX motif abolish Ras signaling and membrane localization [14]. Crystallographic and mutagenesis studies have identified the highly flexible switch regions as critical for the association of Ras with effectors, GAPs and GEFs [15,16,17,18,19]. Switch I includes α helix I and loop 2 (residues 25 - 40[2]) and switch II contains loop 4 and α2 (residues 60 - 75). Sequence alignment of human Ras isoforms and the related Rap 1B highlights sequence variation between Ras and Rap at lobe II as well as the switch regions (Figure 1.2). Rap 1B also associates with the Ras effector Raf at switch I [20]. However, whereas Ras activates Raf, Rap has an inhibitory role which can be reversed by mutating switch I residues to resemble that of Ras switch I [21]. This emphasizes the importance of conservation of lobe I residues amongst Ras isoforms in their ability to associate with a shared set of effectors.

The tertiary structure of Ras isoforms consists of a six-stranded beta sheet and five alpha helices connected by 10 loops [22]. Lobe I contains the functionally important switch regions which undergo a conformational change upon GTP hydrolysis (Figure 1.3) [23]. A magnesium ion is found in the pocket formed by switch I and the P-loop, coordinated by the γ-phosphate of GTP and the switch I residue T35. Multiple studies on oncogenic Ras have identified positions 12, 13 and 61 [24] as the primary sites where activating somatic mutations result in a constitutively active protein characterized by a reduced GAP action and/or intrinsic GTPase activity. [8]

---

[2] Switch I and II have various descriptions on the range of residues however, they both encompass the α-helices and loops mentioned. The residues indicated are what we have used to identify switch I and II for this study.
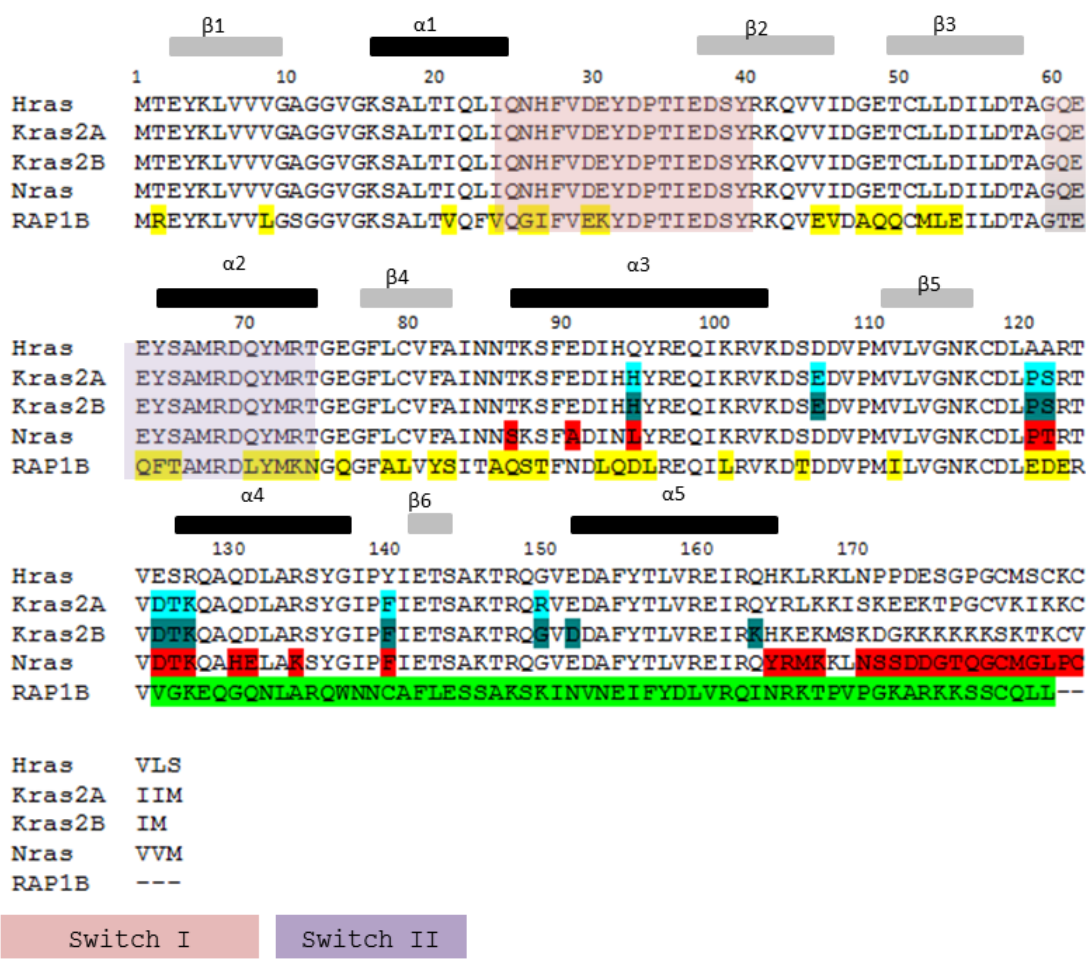
**Figure 1.2** Sequence alignments of human Ras isoforms and the related protein RAP1B. Switch regions are colored in pink and purple with secondary structures indicated at the top, colored black for α helices and grey for β strands. Cyan , turquoise, red and yellow highlight residues in K-ras 4A , K-ras 4B , N-ras and Rap1A respectively that differ from H-ras in sequence. Residues in green highlight the sequence variability of Rap1B on lobe II.
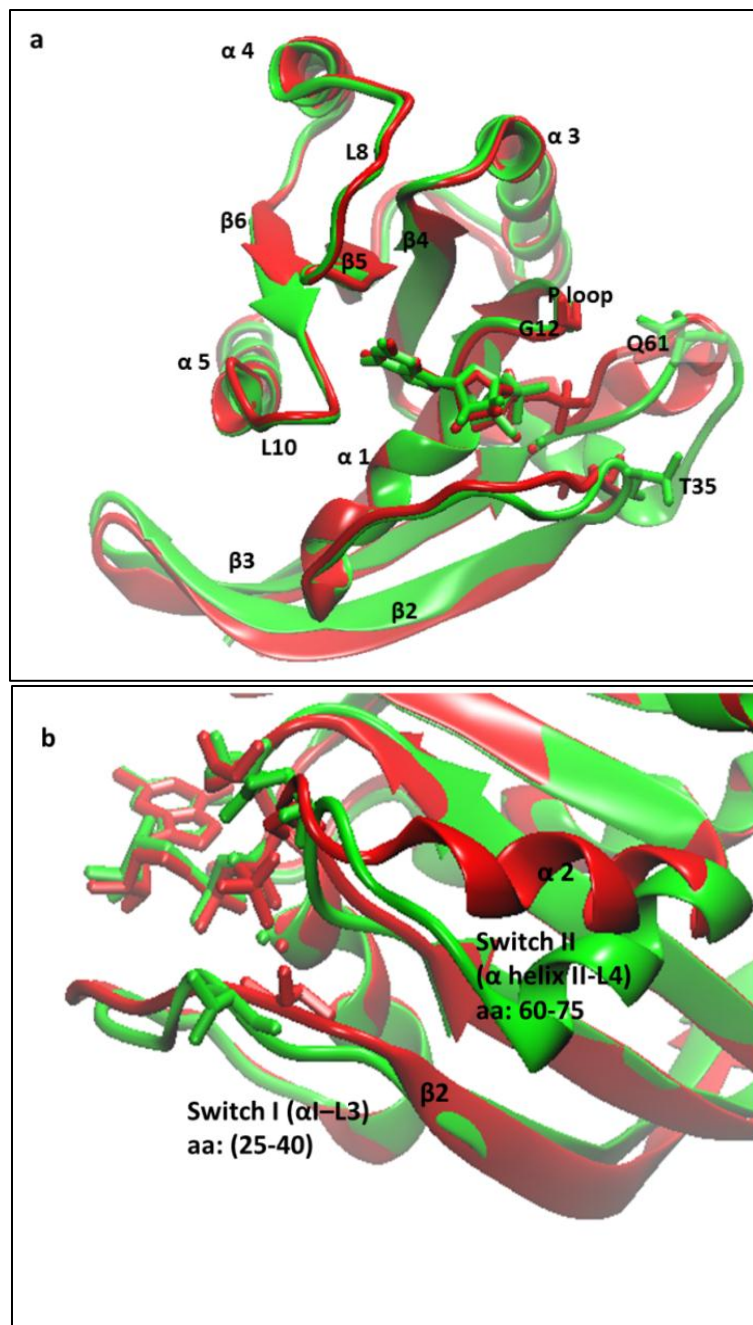
**Figure 1.3:** (a) Superimposition of Ras structures in the active (red) and inactive (green) states based on pdb ids 1QRA and 4Q21, respectively. α helices and β sheets are labeled, as are residues 12 and 61. GTP and GDP are depicted in licorice. (b) The figure in (a) is rotated to highlight differences in the switch II conformation.

## 1.3 Ras Conformational Switching

Although Ras proteins function by cycling between Ras·GTP and Ras·GDP conformational states, NMR studies have shown that GTP Ras exists in two major conformational sub-states termed state I and state II [25]. State I is assumed to be a weak effector binding conformation characterized by the loss of interaction between the GTP γ-phosphate and T35 OH, which results in a marked displacement of switch I from the nucleotide [26]. Since, the interconversion between states I and II is accounted for by the change in interactions of T35 with $Mg^{2+}$ and T35 with the γ phosphate, mutants of T35, such as T35S and T35A, predominantly assume the state I conformation. The former weakly populates state II upon addition of effectors [27]. GTP hydrolysis is greatly reduced in state I, however in some cases addition of effectors results in a shift to state II and an increase in the GAP-assisted GTP hydrolysis rate [25]. Based on these observations one may hypothesize effector binding involves a combination of conformational selection and induced fit mechanisms. Further studies have shown that both point mutations of the nucleotide (i.e. GTP analogues) can shift the conformational equilibrium to state I [28,29,30]. Moreover, Ras·GDP and state I Ras·GTP have a higher affinity for GEFs whereas state II Ras·GTP does not interact with GEFs [31]. The rate limiting step in Ras conformational switching has been proposed to be the dissociation of GDP from Ras by GEFs [32]. Although nucleotide free Ras may be very dynamic and unable to associate with modulators or GAPs, a recent study showed that nucleotide free Ras interacts with a class II phosphatidylinositol 3-kinase beta in an inhibitory manner, which is not observed for Ras·GTP [31]. Summarizing these observations Figure 1.4 illustrates our updated view of Ras conformational cycling.
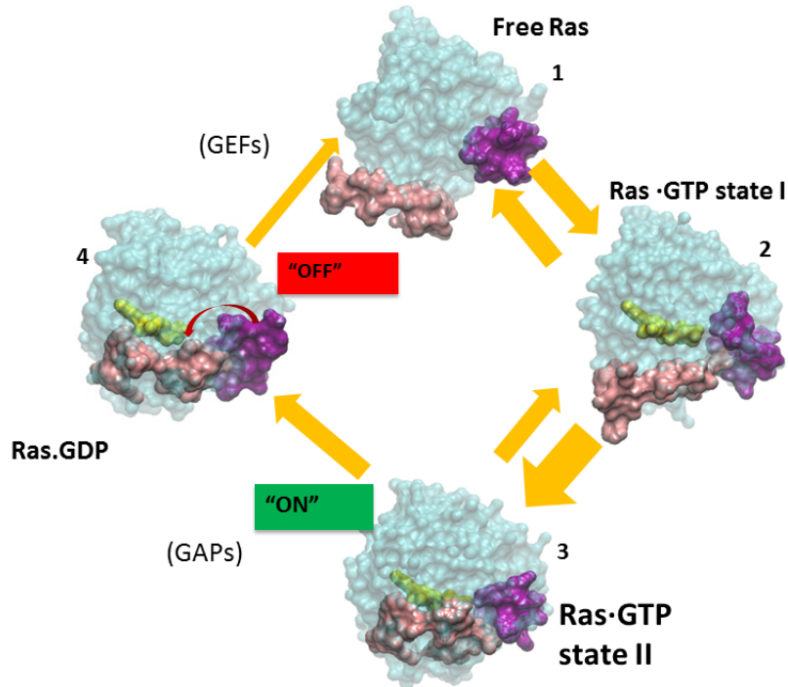
**Figure 1.4:** Illustration of Ras conformational switching based on pdb ids 1BKD (1)[3] , 3KKN (2), 1QRA(3) and 4Q21(4). Switches I and II are in pink and purple, respectively, and the nucleotide is shown in yellow. One can clearly see that the switch regions undergo large conformational changes, with nucleotide free Ras characterized by wide open switch I/II whereas in Ras·GTP state II the switches are closed over the nucleotide.

## 1.4 Isoform Specificity and Functional Roles for Ras isoforms.

Although Ras isoforms have highly conserved catalytic domain and their expression ubiquitous and broadly conserved across eukaryotic species, there has been overwhelming evidence that their biological activities are not redundant. Firstly, H-ras and N-Ras have been shown to be dispensable for development in mice, whereas K-ras 4B (from here on K-ras) knockout results in embryonic lethality. Moreover, these studies revealed that K-ras is sufficient for development in the absence of H-ras and N-ras [33,34]. Besides the critical role

---

[3] Labeled on the diagram for easier reference

of K-ras for development, H-ras and K-ras differ in their ability to activate different effector pathways including the Rac, Raf and PI3K pathways [35,36,37]. Additionally, the tumor suppressor and Ras effector RASSF5/NORE-1 and RASSF2 bind strongly to K-Ras but only weakly to N-Ras and H-Ras [38,39]. Finally calmodulin modulates K-ras·GTP function but not H-ras or N-ras [40].

**Role of the HVR in Isoform Specificity**

Much of the previous work on Ras isoform specific signaling have focused on the role of the HVR and its differential posttranslational lipid modification, and the resultant effect on membrane localization and effector recruitment [13,41,42]. Consequently, the majority of investigations into Ras isoform specific signaling have focused on Ras nanoclustering and distribution on membrane domains. Indeed, analysis of Ras micro-localization in the membrane shows that activated H-ras and K-ras reside in non-overlapping cholesterol–independent domains stabilized by galectin 1 for H-ras and galectin 3 for K-ras whereas inactive H-Ras localizes to cholesterol-dependent domains [13,43,44]. Additionally, Raf-1 is preferentially recruited to K-Ras-GTP nanoclusters and retained in these clusters but not retained in H-ras nanoclusters [42].

**Is there a role for specific conformational dynamics at the catalytic domain?**

While there is substantial evidence that clearly shows the role of Ras localization and orientation in the membrane to explain isoform specific signaling, the possible role of isoform specific dynamics at the catalytic domain has not been well studied. Furthermore, there is a growing body of evidence that suggests a role for isoform specific dynamics of K-ras and H-ras in modulating function. Moreover, previous biochemical and mutational

studies have shown that the catalytic domain may play a role in specificity towards effectors [37,45]. Firstly H-ras has been shown to bind Raf-RBD with slightly higher affinity than K-ras [46]. Meanwhile, *in vitro* biochemical studies revealed that these isoforms exhibit specificities in their ability to activate different effector pathways, with K-ras being a more potent activator of Raf independent of Raf-recruitment to the membrane, while H-ras is a more potent activator of PI3K [37]. Also, specific H-ras mutations are capable of shifting the specificity towards specific effectors (Table 1.1) [47]. Moreover, the Ras GEF Ras-GRF activates H-ras but not N-ras or K-ras 4B and that palmitylation was not required for the specificity of Ras-GRF to H-ras [48].

**Isoform specificity in diseases**

Genetic studies revealed that the occurrence of Ras mutations in tumors are isoform specific, with K-ras being the most frequently mutated isoform in in pancreatic, colon and lung cancer whereas H-ras has a higher occurrence in bladder carcinomas and N-ras in neurological cancers [49]. Surprisingly, also the location of mutations on a specific isoform varies in frequency and tissues it is expressed in [50]. For example, oncogenic G12V substitution accounts for over 80% of K-ras mutations, almost double that of N-ras mutations at position 12. There is a relatively low occurrence of Q61 mutations in K-ras yet H-ras and N-ras are found mutated more than 40% and 60% at position 61, respectively. In addition, specific point mutations in K-ras may affect effector specificity since more recent studies have shown that the oncogenic potential of K-ras G12D in pancreatic tumors is through activation of the PI3K pathway rather than C-Raf [51]. Another study revealed that G12D K-ras bound to Raf was only about 2% of the total K-ras [52]. Recently, Ras mutants have also been found in developmental diseases that share the characteristic phenotype of a group of diseases known

as Neuro-Cardio-Facio-Cutaneos Syndromes (NCFC's) [53,54]. Within this class of diseases, germ line H-ras mutations at position 12[4] are consistent with the phenotype of Costello syndrome, whereas widespread expression of oncogenic K-ras G12D is not tolerated and results in embryonic lethality [50,55,56]. Furthermore, K-ras mutants are not found in Costello syndrome but appear in other NCFC's.

| H-ras mutant | Location | Specific effector[5] |
|---|---|---|
| G12V/T35S<br>T35S | Switch I | Raf |
| G12V/D38E | Switch I | Raf |
| G12V/D37G | Switch I | Ral |
| G12V/Y64G | Switch II | Raf/Ral-GDS |
| G12V/Y40C | Switch I | PI3K |

**Table 1.1**: Ras effector specific mutants

**Motivation and Specific Aims of This study**

Conformational selection postulates that proteins exist in many different conformational states around the average structure [57]. At equilibrium, the conformational states that are populated when bound to a particular ligand are part of a conformational repository in the absence of the ligand [58]. In the case of Ras, accelerated molecular dynamics simulation and other studies have revealed that, in the absence of GTP or GDP, H-ras can sample structures that resemble the GDP and GTP state conformations [59]. Moreover, GDP Ras is able to associate with a mutant Raf RBD but X-ray analysis of the complex shows a conformation

---

[4] G12S mutation is the most common; G12V, G12D and G12A were also reported.
[5] Effector specific mutant ras maintains the ability to associate with only these effectors

similar to that of Ras·GTP [60]. Though GDP·Ras binds Raf with a much lower affinity than GTP·Ras, this finding clearly demonstrates that in each of the major sub-states there exist conformations that can be selected for association with ligands or effectors[6]. The specificity of the Ras mutants T35S and Y40C towards interactions with Raf and PI3K further suggests that there must be distinct conformational populations in these mutants that favor interaction with a specific effector. Since neither residue 35 or 40 have been implicated in direct interaction with PI3K or Raf RBD, one may surmise that these mutations alter dynamics instead [15,61]. This is true for Y40C H-ras, which, although PI3K specific, can still associate with Raf under very high (non-physiological) concentrations of Raf RBD [28].  In this work, we aim to assess the dynamics of Ras in the GTP bound state to probe specific dynamical and conformational differences between H- and K-ras isoforms and between wild type mutant Ras proteins. The first specific aim of the study is therefore a detailed investigation of Ras dynamics through all-atom molecular dynamics simulations of the catalytic domain. The second aim is to assess the specific role of conformational dynamics and residue interactions within each sub-state and how these might be affected by point mutations. ***Our overreaching hypothesis is that sequence variation on lobe II (Figure 1.5) of Ras alters dynamics and leads to differential preference for different effectors or modulators.***

---

[6] The Raf A89K mutant was used in the mentioned study because of its higher affinity for Ras.
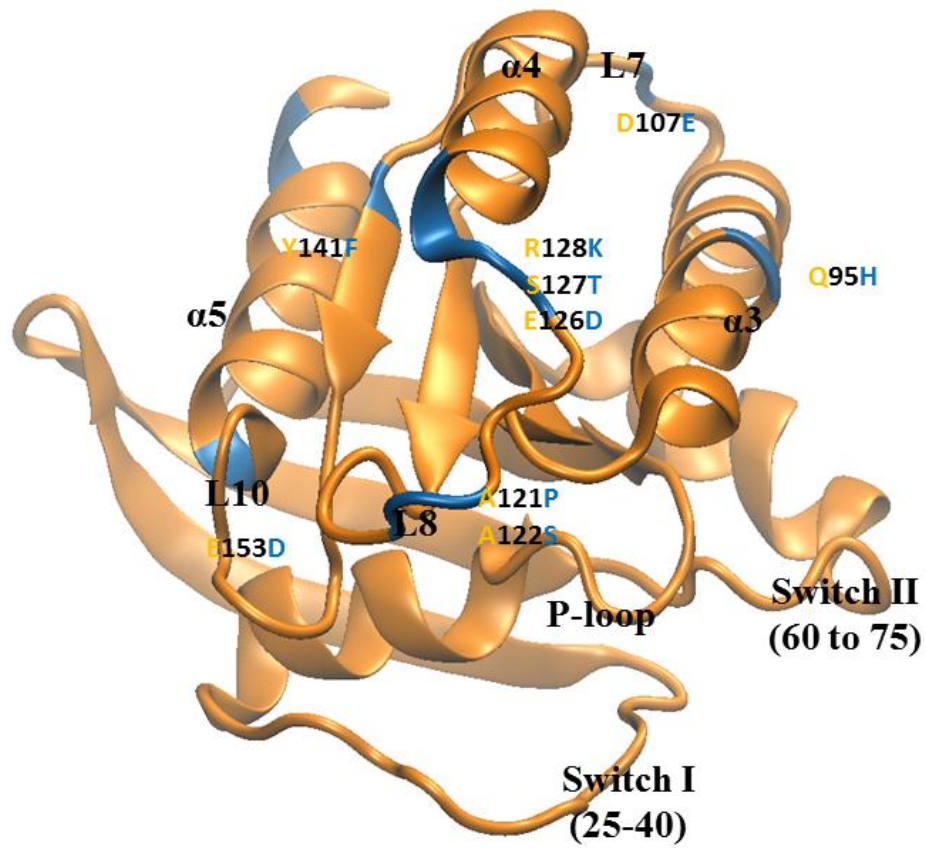
**Figure 1.5:** Cartoon representation of H-ras catalytic domain (pdb 1QRA) with the locations of sequence variation between H-ras and K-ras colored in blue and labeled in orange for H-ras and blue for K-ras.

# CHAPTER 2

## Overview of Molecular Dynamics Simulations and Key Trajectory Analysis Techniques

In order to examine the various conformational states of Ras proteins we have utilized molecular dynamics (MD) simulations to produce an ensemble of structures (conformers). A comprehensive analysis of the MD-derived trajectories was carried out utilizing several analysis techniques. In this Chapter, I will provide the reader with a general overview of the theoretical basis of molecular dynamics simulations as well as principal component analysis (PCA) and other multivariate data analysis techniques used to characterize Ras dynamics and structural perturbations.

### 2.1 Molecular Dynamics

Molecular dynamics is a computational method that is used to describe the motions of atoms and molecules. MD relies on concepts from statistical mechanics and thermodynamics to study biomolecular dynamics at the atomistic level, and is used to observe global (large-scale) fluctuations as well as local motions and specific effects of external perturbation of protein conformations. In an MD simulation, each atom is considered to be a point mass and its motion is determined by the forces exerted upon it by all other atoms as determined by Newton's equations of motion in classical dynamics [62,63]. MD allows us to explore the dynamics of proteins *in silico* on timescales inaccessible to conventional *in vitro* or *in vivo* methods.

**Generating an MD trajectory**

In order to generate a MD trajectory starting atomic coordinates from X-ray crystallography, NMR or homology modeling, as well as assignment of random atomic velocities are needed. Newton's equation describes the force $F_i$ acting on particle $i$ in terms of the product of the mass ($m$) and acceleration ($a$) of the atom:

$$F_i = m_i a_i \qquad (2.1)$$

Force can be described as a gradient of the potential energy ($V$) ,

$$F_i = -\nabla_i V \qquad (2.2)$$

and the derivative of the potential energy is related to the change in atomic position as

$$-\frac{dV}{dr_i} = m_i \frac{d^2 r_i}{dt^2}. \qquad (2.3)$$

Acceleration is therefore as the derivative of the potential energy with respect to position, $r$.

In an MD simulation, the protein is described as a series of charged points (atoms) linked by springs (bonds). At each step during the simulation, the forces on each atom are computed and the atomic position and velocity are updated according to Newton's laws of motion. These forces are determined from the force field, which is a collection of parameters that represent both bonded and non-bonded energy terms [64].

A typical force field has the following functional form:

$$V = \sum_{bonds} \frac{a_i}{2}(l_i - l_{i0})^2 + \sum_{angles} \frac{b_i}{2}(\theta_i - \theta_{i0})^2 + \sum_{torsions} \frac{V_n}{2}(1 + \cos(n\omega - \gamma)) +$$

$$\frac{1}{2}\sum_{i=1}^{N}\sum_{j\neq i}^{N} 4 \in_{ij} \left[ \left(\frac{\sigma_{ij}}{r_{ij}}\right)^{12} - \left(\frac{\sigma_{ij}}{r_{ij}}\right)^{6} \right] + \frac{1}{2}\sum_{i=1}^{N}\sum_{j\neq i}^{N} \frac{q_i q_j}{r_{ij}} \qquad (2.4)$$

The first three terms represent the bonded energy terms defined oscillations about the equilibrium bond length, angle and torsion, while the last two terms represent the non-bonded energy terms described by the Lennard-Jones potential and the Coulomb equation. The Lennard-Jones potential is weakly attractive at short distances for two uncharged molecules, but is strongly repulsive when they approach too close. The Coulomb potential describes the interaction between two point charges. Using the relationship, $F_i = -\nabla_i V$, the forces acting on the atoms are calculated and the atomic positions can be updated through the numerical integration of $F_i = m_i a_i$.

An major advantage of MD over other methods is that it is one of the most detailed molecular simulation methods which computes motion of individual atoms [65]. The limitations include the limited size of conformational space that can be sampled and the accuracy of the force field. The problem of sampling limitation is the most severe and is coupled with the size and complexity of the system to be simulated. This sampling issue is currently being addressed by several computational groups [66].

The use of an integrator scheme such as Leapfrog or the Velocity Verlet algorithms assumes the positions, velocities and accelerations can be approximated by a Taylor series expansion. NAMD uses the Velocity Verlet to advance the positions and velocities of the atoms in time, which computes the forces of the atom as a function of position, and does not involve the explicit calculation of the velocities [67]. Additionally in order to reduce the cost of evaluating the forces due to long range electrostatics, NAMD utilizes a multiple time-stepping scheme. Through the use of specific cutoff distance, the forces on local and long range electrostatic interactions within the cutoff is computed while long range interactions beyond the cut-off are computed less often

Periodic boundary conditions are a method of simulating many atom systems and improving computational efficiency by eliminating the behaviors near the walls of the system. The bulk of the system is assumed to be composed of the primary cell which is surrounded by its mirror image on all sides. Utilizing periodic boundary conditions allows any atom that leaves a simulation box from one side to enter from the other since molecules are free to diffuse within the system [68].

## 2.2 Analysis of Molecular Dynamics Trajectories

In order to correlate the functional relationship with the structure it is imperative that we study the dynamics which is correlated with conformational changes and flexibility crucial for protein function.

A variety of analyses were performed on the resulting molecular dynamics trajectory using the programs VMD [69], Bio3d in R [70] and Wordom [71]. The first step involved removal of the waters and alignment of the Cα coordinates of the atoms to the core atoms of the protein using the Kabsch algorithm [72], which computes the rotation matrix that minimizes the RMSD. Alignment of the structures is necessary to remove translational motions inside the simulation box as the protein is free to diffuse.

**Root Mean Square Deviation analysis (RMSD)**

Root mean square deviation (RMSD) is used as a measure of the difference between two sets of values. Here the RMSD of each atom is computed with respect to a reference structure, over the time course of the simulation. In this way the RMSD can give valuable information about the extent of the conformational difference between two structures. Furthermore a plot of the RMSD of a trajectory is useful to gauge equilibration of the system or to identify the

time points of conformational changes for further analysis. In our RMSD analysis, each frame of the trajectory was first fitted on a reference structure based on the core atomic coordinates to remove translation and rotation of the protein. Since RMSD is dependent on the atoms used for fitting and for our purposes only Cα atoms were used as a representation of the protein backbone.

$$RMSD = \sqrt{\frac{1}{N}\sum_{i=1}|x_i\ (t1) - x_i\ (ref)|} \tag{2.5}$$

In equation 2.5, N is the total number of atoms and $x_i(t1)$ is the position (x) of atom *i* at time t1 and $x_i(ref)$ is the reference  position.

**Root Mean Square Fluctuation (RMSF)**

While crystal structures provide valuable information about the average structure of a protein, MD simulations allow us to investigate the dynamic fluctuations around the average structure. While the the RMSD is a way of identifying the fluctuations of different conformers over time, the RMSF serves as a means of describing the individual atomic fluctuations.

The mean square fluctuation gives the deviation of each atom (Cα most widely used) averaged over time. This is similar to the B-factor in crystallographic studies, which attempts to show the dynamics of individual atoms. The RMSF of atomic positions is measured from the structure . Flexibility is of great importance to a protein's biological functioning, stability, and conformational behavior directly affecting the conformational changes within the time period sampled.  The RMSF is given as

$$RMSF = \sqrt{\frac{1}{T}\sum_{j=1}^{T}((xi_j) - \overline{xi})^2} \tag{2.6}$$

$\overline{x}$ is the avergae position of atom i over the time T (or T number of structures)

**Dynamic Cross Correlation (DCC) Analysis:**

Dynamic cross correlation is a useful method to capture and characterize correlated atomic motions, thereby defining long-range allosteric couplings within a protein. The theory behind DCC lies in the fact that residues of a domain (or region) move in concert with one another based on their atomic cross correlation coefficients. These correlation coefficients are determined from the positional vectors. In analyzing time covariance and the normalized covariance or cross correlations of atomic fluctuations, we can gather information about the correlated atomic motions [73]. For the displacement vectors of atoms i and j ($\Delta r_i$ and $\Delta r_j$), the covariance *c(ij)* is given by the dot product of the ensemble average $< >$ of these displacements.

$$c(ij) = <\mathbf{\Delta r_i} \cdot \mathbf{\Delta r_j}> \tag{2.7}$$

The mean square atomic fluctuation $<\Delta r^2_i>$ is the diagonal of $<\Delta r_i \cdot \Delta r_j>$ .The normalized covariance, $C(i,j)$ is the cross correlation of …… and is given by:

$$C(i,j) = \frac{<\Delta r_i \cdot \Delta r_j >}{<\Delta r_i^2>^{1/2} <\Delta r_j^2>^{1/2}} \tag{2.8}$$

In a molecular dynamics trajectory the covariance is computed over time by estimating the ensemble average over a set of discrete time points for a pair of atoms *i* and *j*. In the current study we employ dynamic cross correlation analysis to identify the communication pathways across Ras isoforms and mutants.

18

**Principal Component Analysis (PCA)**

MD essentially yields multivariate data set, where many of the variables (atomic coordinates) are correlated or dependent on each other. A multivariate analysis tool is needed to investigate the most relevant collective fluctuations. One such technique that has gained popularity in analyzing protein trajectory data is Principal Component Analysis (PCA), which reduces a multidimensional data set to a lower dimensional data. In applying PCA to molecular dynamics trajectories the goal is to reduce the data such that it highlights the independent variables (atomic coordinates) to explain the conformational changes of interest. In some instances it is also useful to apply PCA using dihedral angles instead of atomic coordinates, however a transformation from angular coordinates to $\phi_n$ to Cartesian coordinate space $\{xn=\cos\phi\ n\ ,\ yn=\sin\phi n\ \}$ must be performed [74].

The application of PCA involves first the diagonalization of the covariance matrix of atomic positions and then identification of an orthogonal set of eig envectors, which describe the direction of maximum variation in the data set. The eigenvectors of the covariance matrix are the axes of maximum variance. The principal components (PC's) are dot products of the original variables with a weight $\alpha$ that are uncorrelated and ordered such that the first few PC's retain the greatest percentage of the variance that was present in the original variables.

To reiterate this concept, we can consider an example of a vector **x** with *p* random variables. A linear $\alpha'_1x$ function of the elements of **x** that has maximum variance where $\alpha_1$ is a vector of *p* constants

$$Z_1 = \alpha_{11}x_1 + \alpha_{12}x_2 + \ldots + \alpha_{1p}x_p = \sum_{j=1}^{p} \alpha_{1j}x_j \qquad (2.9)$$

The weights in this case are the eigenvectors of the covariance matrix, and are interpreted to reveal the per-residue contribution to the variance (Figure 3.2) .The second PC ($z_2 = \alpha'2x$) has the properties of having the second highest variance but is uncorrelated with $z_1$. This lack of correlation between the PCs is very important in interpreting the data since the indices of the PC's can be interpreted as variance in different dimensions in the original data. The original data is then projected onto the weights ($\alpha$) of the associated principal components and these are plotted against each other.

## 2.3. Salt bridges, Hydrogen Bonds and Hydrophobic Contacts

A contact map was made to select residue-residue contacts based on an inter-atomic distance cutoff of 4 Å between the side chains of atoms. The 4 Å distance cutoff is sufficient to identify atomics interactions that may be electrostatic and hydrophobic interactions between residues. After the initial conformer analysis, we utilized this map to identify unique residue – residue contacts for each system.  Hydrogen bonds (H-bonds) exist between a polar H atom (such the amide hydrogen, NH) and an unshared pair of electrons in an electronegative atom such as oxygen and nitrogen.  For instance, since an amide N atom is electronegative the H on the NH atom becomes partially positive or has a positive dipole this atom is then attracted to another electronegative atom such as an O or N with an unshared pair of electrons. The energy of a H-bond can be up to 4-13 kJ mol$^{-1}$ [75]. Therefore, hydrogen bonds contribute greatly to the overall stability of proteins [76]. To identify H-bonds of interest we used the VMD H-bond plugin which identifies H-bonds based on a donor-acceptor distance cutoff of 3.0 Angstrom and a donor-H-acceptor angle cutoff of 20.0 degrees (Figure 2.1).
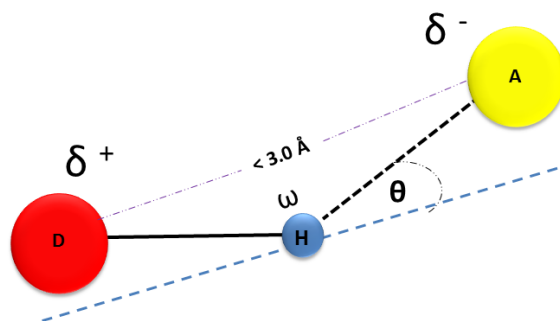
**Figure 2.1:** Illustration of the hydrogen bond (H-bond) criteria used. A distance of less than 3Å between the donor (D) and acceptor (A). The angle θ is less than 20 degrees since the H-bond is almost linear and ω is less than 180 degrees.

Salt bridges are formed by the electrostatic interaction between oppositely charged amino acids mainly Aspartate and Glutamate with Lysine and Arginine, when they come within a certain distance to experience an electrostatic attraction. They have been shown to play important roles in protein function including molecular recognition, allosteric regulation, flexibility and thermostability [77]. The roles of salt bridges in protein stability have been a widely debated issue. Mutational studies aimed at disrupting salt bridges in proteins have indicated that they actually contribute less to protein stability but instead have greater contributions to the burial of hydrophobic side-chains to form and stabilize the core. However studies on surface salt bridges have revealed that altering certain salt bridges can have a substantial effect on protein stability, with a possible advantage to promote protein stability at higher temperatures [78,79]. Salt bridges have been found to play critical roles in conformational changes. For example, rhodopsin cycling between inactive and active states involves the formation and breakage of a salt bridge between two helices [80].

In our systems we used a distance cutoff of 3.2 Å between the side chains of either oxygen of acidic amino acids and the nitrogen of basic residues to define a salt bridge. Figure 2.2 illustrates a salt bridge formed between K5 and D54 in the Ras crystal structure. This salt

bridge may a have functional role since mutations of the K5 residue to N have been

implicated in colon cancer and developmental diseases. [81,82]
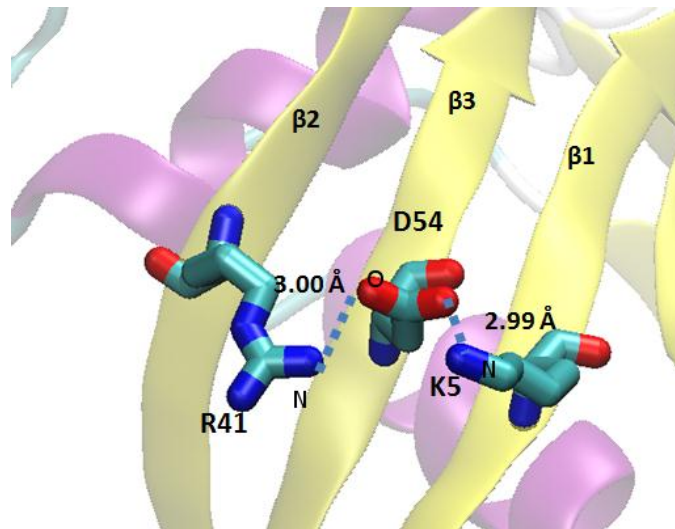


**Figure 2.2**: Salt bridge formed between two β strands on H-ras (pdb 1QRA). Nitrogen and Oxygen atoms involved in the salt bridge are labeled as N and O respectively

## CHAPTER 3

## METHODS

**Chapter Overview:**

In this Chapter I will present details of the methods used to assess the conformational dynamics across Ras structures and conformers obtained from molecular dynamics simulations. Firstly an overview of the simulation details will be presented, followed by Principal Component Analysis (PCA) that was used to explore the various conformational states of Ras crystal structures[7] in the nucleotide bound state and in complex with effectors/modulators. I will then discuss the application of PCA to analyze the MD trajectories and expound on the clustering analysis used to detect major conformational clusters for a detailed analysis. Lastly a brief definition of the parameters used to characterize the conformational states of Ras obtained from MD simulations is presented.

**3.1 Molecular Dynamics Simulations of Ras.**

**Rationale**

In order to identify different conformational states for H-ras and K-ras, MD simulations were carried out on the catalytic domain (residues 1-166 or 1- 167) of these isoforms, with bound GTP and $Mg^{2+}$. NMR analysis of full length H-ras have reported that the biochemical properties of the protein are retained in the truncated protein that possesses just the catalytic-domain, hence analysis of the catalytic-domain is sufficient to explore Ras dynamics that may perturb its function [83].

The H-ras T35S mutant (T35S) was also studied because it retains the ability to associate with Raf but not PI3K [84]. Specifically, through analysis of T35S and a comparison with H-ras and K-ras we hope to either gain insights into Ras dynamics that may favor interaction

---

[7] Obtained from the PDB data bank.

with Raf or interfere with its association with PI3K. We included the T35A H-ras mutant (T35A) because it predominantly exists in state I and does not interact with any known effectors of Ras, hence the conformations sampled by this mutant will be considered non-favorable for effector/GAP interactions [26].

Crystal structures of Q61H H-ras and K-ras oncogenic mutants in complex with GNP[8] and $Mg^{2+}$ were retrieved from the PDB data bank. These simulations were run to satisfy two requirements.

1. Validate the structural differences between H-ras and K-ras since no WT K-ras structure is currently available.

2. To answer the question: Do specific mutations perturb the conformational dynamics of Ras isoforms differently?

**Simulation Details**

Production simulations were commenced after equilibration and minimization of the coordinates of the appropriate crystal structures from the Protein Data Bank (PDB)[85]. The details of each system are listed in Table 3.1, along with corresponding mutations and starting structures. Missing hydrogens were built and the protein structure file was created using the psfgen plugin within VMD [69]. The systems were prepared by first solvating the protein in a water box of padding 10 Å around the molecule and a cubic box of dimensions 60.43 x 60.43 x 60.43Å$^3$ . Crystal waters were retained and the systems were checked to remove water clashes (i e. waters within 2.4 Å of the protein) and subsequently neutralized by the addition of $Na^+$ and $Cl^-$ ions. Histidine residues were set to neutral.

---

[8] The GNP was replaced with GTP in simulations.

The resulting systems were subjected to energy minimization with a time step of 1fs using the conjugate gradient method, which consisted of 2000 steps with harmonic restraints placed on the heavy atoms (k = 4 kcal/mol/$\text{Å}^2$) and another 2000 steps with the harmonic restraints turned off. The minimized systems were then slowly heated to a temperature of 310K in 50000 steps, and finally equilibrated with constraints of 4.0 kcal/mol/$\text{Å}^2$ applied to the backbone atoms, which was subsequently decreased 25% in four steps to 0 over 0.7ns.

After initial energy minimization and equilibration, production simulations were performed at constant temperature (310K) and pressure (1atm) with a 2fs time step using the NAMD engine [86] and CHARMM27 force field [87]. The SHAKE [88] algorithm was employed to constrain bonds involving hydrogen atoms.

Trajectories were written out every picosecond. Periodic boundary conditions with full Particle-Mesh Ewald (PME) electrostatics [89] were used with  a non-bonded cutoff of 8.5Å and 10Å for non-bonded list update. Each simulation was run for at least 400ns, which is sufficient to examine collective motions including hinge bending, which occurs on the $10^{-11}$s to $10^{-7}$s time scale, and loop motions that occur on the $10^{-9}$ to $10^{-5}$s  time scale [90,91]. The total simulation time was 2.9 μs.

Analysis of the trajectories was carried out using a combination of scripts prepared for Bio3d [70]  in R [92], Wordom [71], and VMD. Prior to subsequent analysis all systems were stripped of waters. For PCA and DCCM analysis only Cα atoms were used for analysis and conformers were sampled every 0.1ns.

| Simulation name | Simulation length (ns) | PDB id of Starting Structure | Resolution (Å) | Modification | Residue | Ligand |
|---|---|---|---|---|---|---|
| H-ras | 550 | 1QRA | 1.6 | - | 1-166 | GTP Mg$^{2+}$ |
| K-ras | 600 | 3GFT | 2.27 | H61 → Q GNP → GTP | 1-167 | GTP Mg$^{2+}$ |
| Q61H (H) | 350 | 6Q21 | 2.4 | GNP → GTP | 1-166 | GTP Mg$^{2+}$ |
| Q61H (K) | 400 | 3GFT | 2.27 | GNP → GTP | 1-167 | GTP Mg$^{2+}$ |
| T35S (H) | 550 | 1XCM | 2.09 | GNP → GTP | 1-166 | GTP Mg$^{2+}$ |
| T35A (H) | 400 | 1QRA | 1.6 | T35 → A | 1-166 | GTP Mg$^{2+}$ |

Total of 2.9 ns

**Table 3.1:** Simulation Details

### 3.2 PCA of Ras x-ray structures

Principal component analysis (described in Chapter 2) is a useful tool for visualizing and classifying protein conformers [93]. However, before PCA can be applied one needs to reduce the number of variables or the structural complexity in order to achieve meaningful results. Therefore, we performed PCA only on the Cα co-ordinates of residues 1-164. To study the various conformational states of Ras, X-ray structures were chosen from the protein data bank including all Ras-GTP[9]/GDP structures deposited to date. Structures that were missing residues within residues 1-164 were omitted and the remaining 65 structures were used to create a conformer plot. All structures were aligned to 3GFT chain A based on the Cα coordinates of the core residues reported by Gorfe et al. in 2008 [94]. A PC plot illustrates conformers in terms of their displacement along a particular PC, which reflects the variance at the residues that contribute to the particular PC. Additionally a plot of the PCA loadings describes specific residue contributions to the displacements in the PCs. Hence we can

---

[9] Structures that are crystalized with GTP analogues are also selected and in some cases effectors and small Molecules. The Mg$^{2+}$ ion is present in many structures.

gauge the conformational differences due to residues that contribute significantly to the variance along particular PCs. In this way PCA and a plot of conformations provides an efficient method of identifying different conformational states.

**PC vs RMSD clustering**

Both PCA and RMSD are useful tools for identifying conformational differences. Hence we can use a difference matrix composed of the pairwise RMSD or significant PC's for distance based clustering. The advantage of PCA in this case is that it allows the identification of critical domains or residues that are important for functional conformational switching. One can easily visualize the different conformational clusters of Ras as a function of conformational similarity at specific regions. The PC plot (Figure 3.1) clearly defines Ras conformational states along PC1 and PC2. These results are in agreement with PCA of Ras reported in Gorfe et Al (2008) [94], however state I conformers had not been included in the previous data set. In Figure 3.1 structures that represent state I conformations (blue), state II (red and orange) and Ras·GDP (green). Cluster selections based on either RMSD or the first three PC's are able to clearly identify these different conformational states. A dendrogram of the crystal structures serves to further illustrate the hierarchal clustering based on RMSD differences (Figure 3.3). The two most conformationally different structures are 3KKN and 2Q21. Also highlighted are T35S H-Ras (3KKN) where there is a significant perturbation at switch I and switch II, as well as the G12V H-ras (2Q21) with distorted switch II (Figure 3.1).

PC-based clustering is able to highlight conformational differences in the switch regions as well as other regions of high variance (Figure 3.3). For example, H-ras in complex with caged GTP (CAG), pdb 1GNQ, is assigned to a separate cluster based on the PCs due to

significant conformational changes in switch I. Also the structure of 3KUD (Ras·GDP-Raf complex) is almost identical to WT H-Ras at switch I but differs at switch II and helix III.
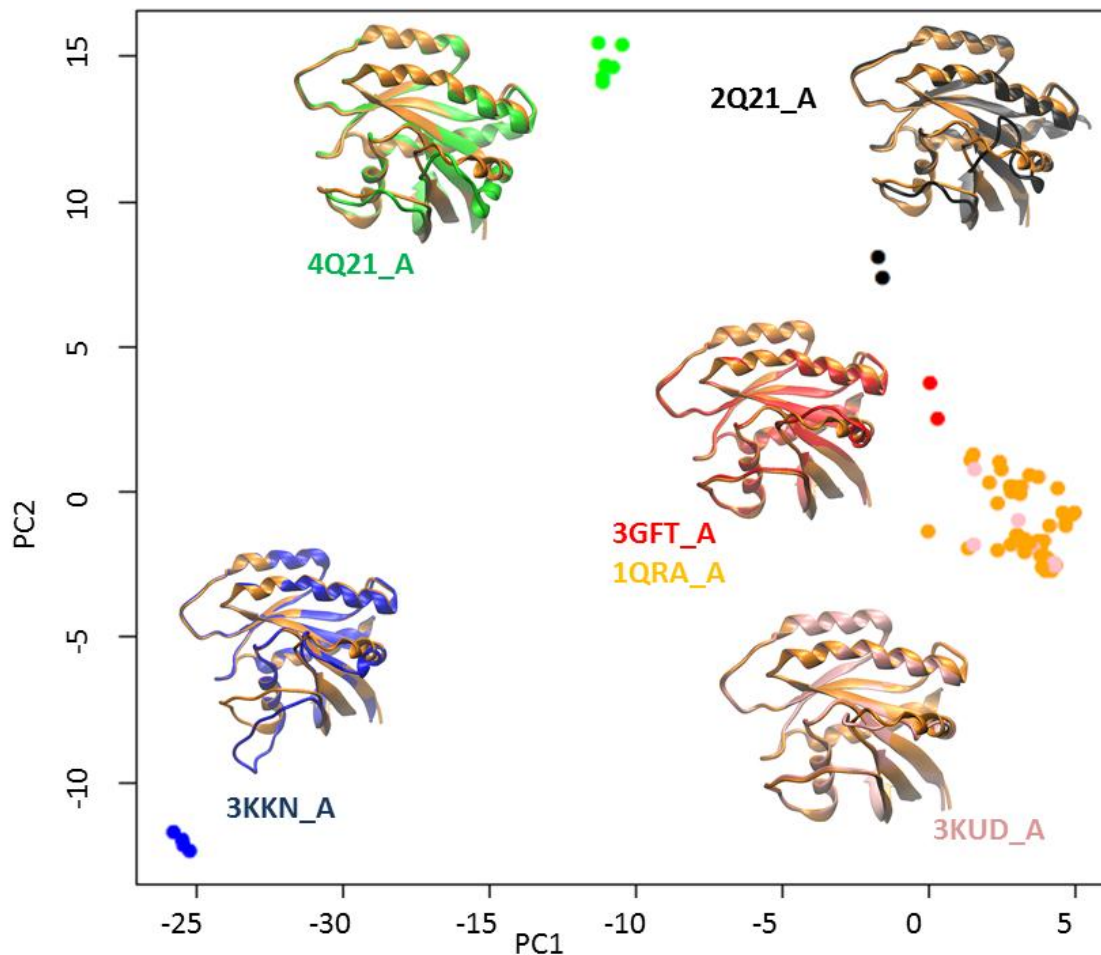


**Figure 3.1** A PCA map of 65 Ras crystal structures colored by RMSD-based clusters. Proteins in colored cartoon representation are representative crystal structures of each cluster colored according to their cluster and aligned against WT H-ras (orange). These structures are labeled by their PDB ID and their difference in RMSD from H-ras GTP (pdb 1QRA) is reported in Table 3.1. Ras state II clusters are colored orange and pink, State I colored blue, GDP and GDP/GTP intermediates green and black respectively.

| PDB ID | STRUCTURE INFORMATION | Δ RMSD from 1QRA (Å) |
|---|---|---|
| **3GFT** | K-ras·GNP Q61H | 1.03 |
| **3KUD** | H-RAS·GDP-RAF COMPLEX(DISTAL SITE) | 0.82 |
| **4Q21** | H-ras GDP | 1.67 |
| **2Q21** | H-ras G12V·GDP | 1.58 |
| **3KKN** | H-ras T35S· GNP | 2.45 |

Table 3.2: The difference in RMSD of the Cα atoms (1-66) from H-ras·GTP ($Mg^{2+}$) 1QRA
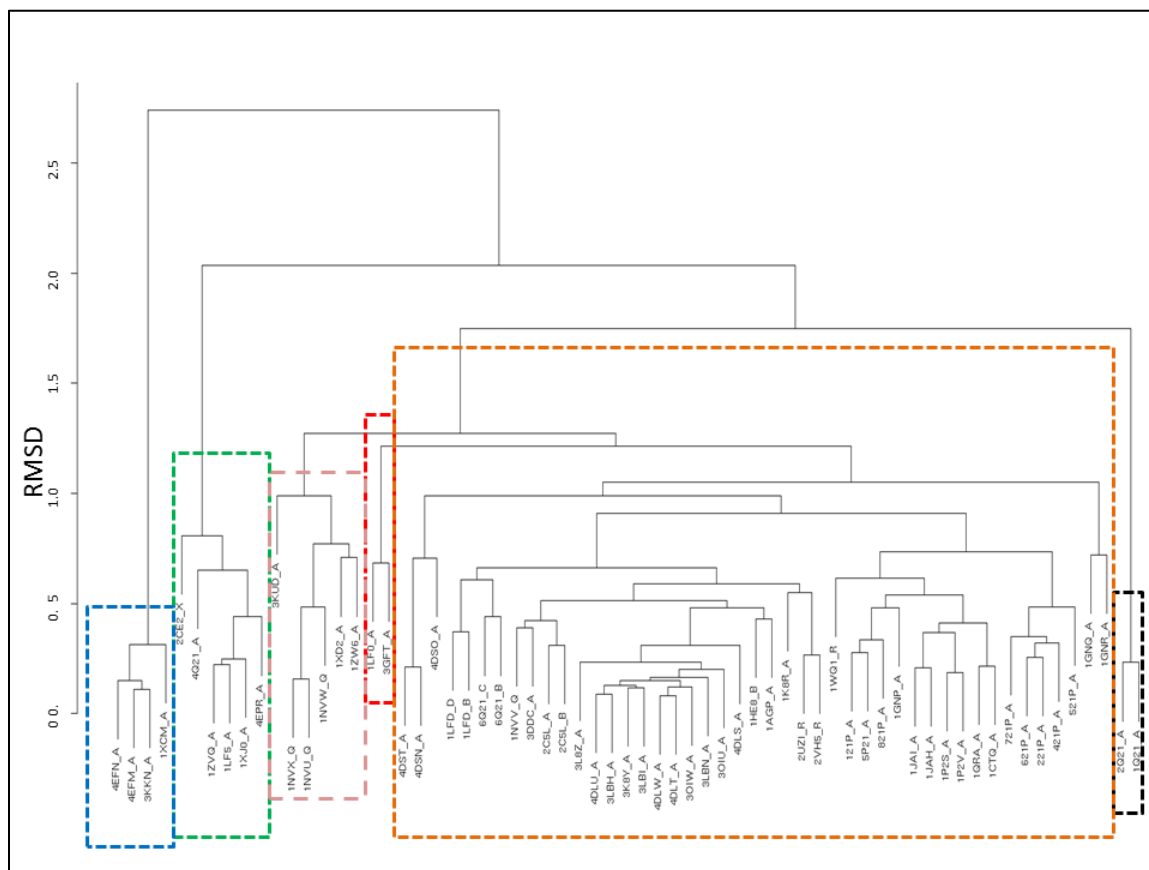


**Figure 3.2:** A dendrogram of Ras crystal structures grouped according to RMSD clusters.
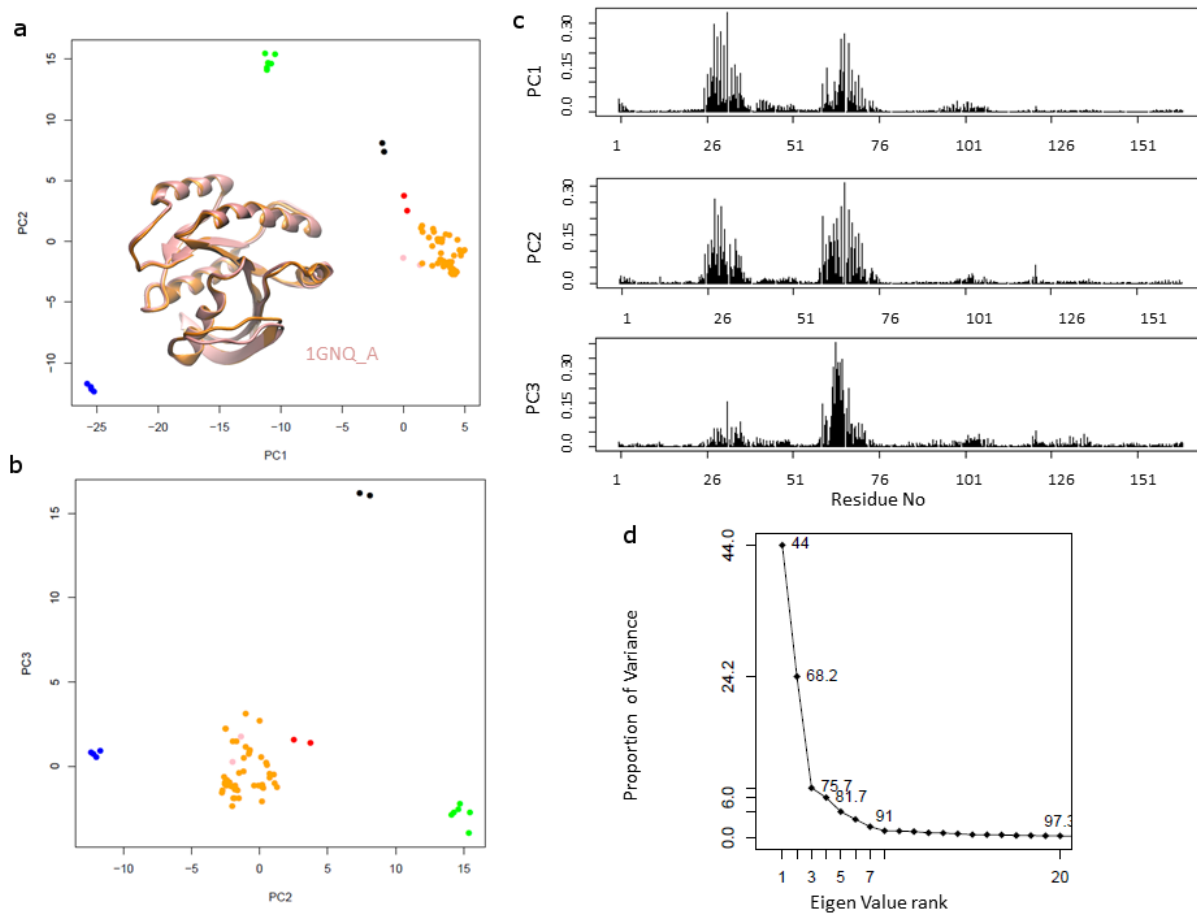
**Figure 3.3:** Conformer plots of Ras crystal structures colored according to PC clusters (a-b). (c) PCA loadings describing residue contributions to each PC. (d) Scree plot showing the contribution of each PC to the total variance.

The PC plot shows a clear distribution of conformational clusters along the major PC's 1, 2 and 3 (Figure 3.3), which account for over 75 % of the variance in the data. The plot of residue contributions to the PCs highlights the switches I and II as the major contributors to the variance (Figure 3.3 (b)). H-ras G60A (1XCM) represents a state I conformation. We can appreciate the separation from the major GTP cluster mainly due to PC1 because of the strong contribution of switch I residues to the variance. Likewise Ras·GDP (4Q21) is separated from the major GTP cluster due to the different orientation of switch II.

**PCA highlights the structural variance of switch I and switch II among sub-states.**

Switch I and II are known to be the most functionally flexible regions in the catalytic domain of Ras. As a result there is a large difference in these regions between state I GTP Ras and Ras·GDP on the one hand and state II GTP Ras on the other. Switch II has a more significant role in determining the variance along PC3. This is emphasized in Figure 3.3 (b), where the plot of PC2 vs PC3 highlights conformational difference of switch II in GDP intermediate structures 2Q21 and 1Q21. Ras·GTP state II conformers are also very well separated along PC's 2 and 3, highlighting a possible role of this region in conformational diversity within state II. Since switch II undergoes a major conformational change upon GTP hydrolysis [23,95], the clear separation of the 2Q21/1Q21 GDP intermediates from the GDP cluster further illustrates the importance of switch II flexibility in Ras conformational switching between GDP "off" state and GTP "on" state, and the impairment of hydrolysis in Ras mutations at the switch regions or P-loop [96].

**3.3 Selection of Conformational Clusters**

To define the similarity between MD conformers, we applied PCA to each trajectory and then performed hierarchical clustering based on a difference matrix created from the first 4 PCs. The number of clusters based on the elbow in the scree plot (Figure 3.4) [97]. This elbow represents the number of PC's that have significant individual contributions to the variance in the data. Significant clusters were chosen to reflect where the contribution of each PC is drastically reduced. In Figure 3.3, after the first four PCs (the elbow), the contribution of each PC to the variance is less than 3.5%. Therefore for H-Ras a total of 9 clusters was representing greater than 10% of the total number of simulated conformers was selected for further analysis. Table 3.3 lists the details of the clusters and cluster population.
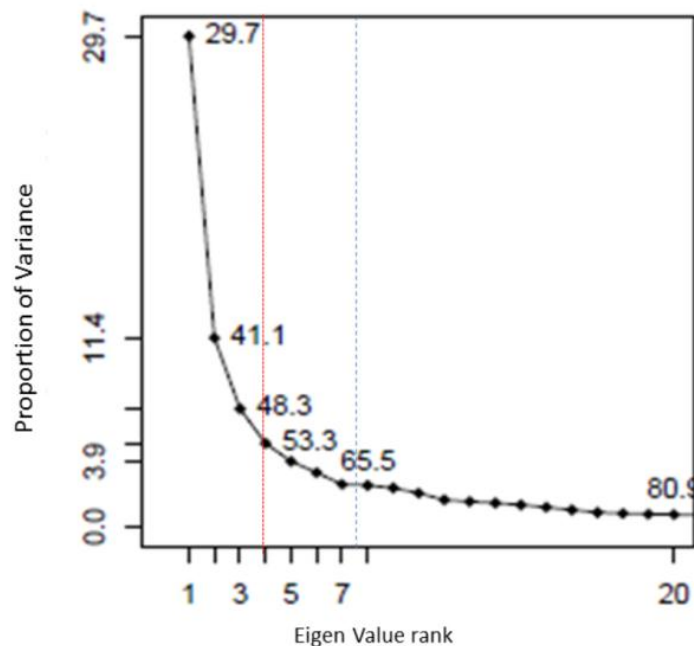
**Figure 3.4:** Scree plot of PCA applied to H-ras conformers. The red line shows the number of PC's used to create the dissimilarity matrix for clustering and the blue line represent the number of clusters.

| System | % Population | | | |
|---|---|---|---|---|
| Protein | Cluster 1 | Cluster 2 | Cluster 3 | All other clusters |
| H-ras | 56% | 35% | 4% | 5% |
| K-ras | 50% | 16% | 7% | 27% |
| T35S | 28% | 16% | 13% | 43% |
| T35A | 46% | 35% | 6.9% | 12.1% |
| Q61H-Hras | 41% | 33% | 19% | 7% |
| Q61H-Kras | 69% | 17% | 7% | 7% |

**Table 3.3:** Conformational Cluster Population Details. Only the first 3 clusters are shown.

**3.4. Identification and characterization of Ras Conformational States**

As discussed in Chapter 1, Ras can adopt two major conformational states when in complex with GTP, a non-effector binding state I and an effector binding state II. Solution NMR analysis of the T35S partial loss of function mutant has shown that the mutant becomes a weak effector binder upon addition of effectors. This is true for other state I mutants except T35A. Previous solution NMR studies have characterized state I and II based on differences in chemical shift values of the $\beta$ and $\gamma$ phosphate due to the distance of the phosphate group from the aromatic ring of Y32 [25]. Furthermore the chemical shifts associated with the $\gamma$-phosphate is accounted for in part by a loss of coordination of the $Mg^{2+}$ ion with the OH of T35, since the electronegative environment surrounding the $\gamma$-phosphate of the GTP can influence the State I/II population [25,29,98]. Hence the loss of the OH of the side chain T35 in the T35S and T35A mutant results in a population shift to state I. [26]. Consequently we utilized the distance between C$\alpha$ atoms of T35 and G12 [10] as well as Y32 and G12 as a metric to discriminate conformations that may be considered state I and state II. Figure 3.3.1 illustrates the position of residues 35 and 32 with respect to their backbone in a state I and state II conformation. The C$\alpha$ distances used for analysis are indicated by dotted lines. To assess the conformational space and dynamics of state I conformers we have studied the T35A [26,29].

---

[10] S35 or A35 for T35 mutants
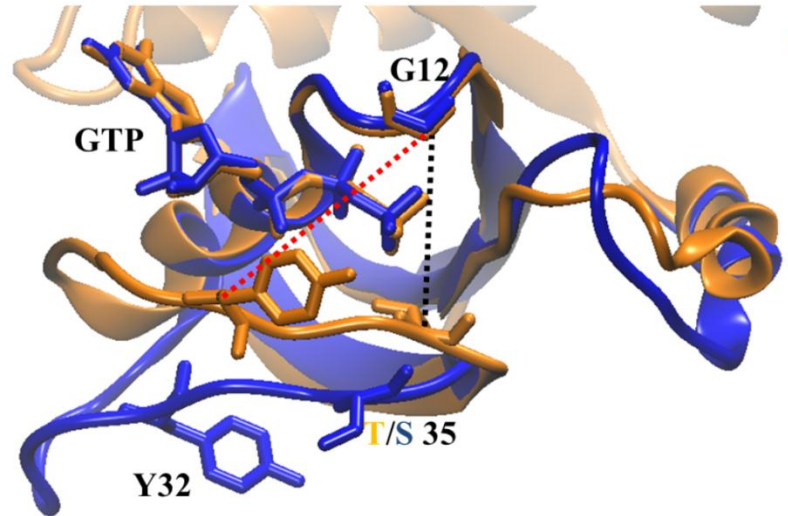
**Figure 3.5:** Orientation of residues 35 and 32 in state II (orange) pdb 1QRA and state I pdb 3KKN.

## 3.4 Cluster selection of MD conformers

Based on the scree plot obtained for PCA carried out on each individual trajectory we have utilized the first four principal components to derive our clusters for subsequent analysis. A distance matrix was created by utilizing the first four principal components which based on the scree plot (Figure 3.4) and also on the pairwise RMSD distances. By utilizing the RMSD clusters, which in most cases encompasses more than 1 PC cluster we are able to identify dynamic elements that would probably assist in the transitioning between different conformations while in the GTP state II state.

# CHAPTER 4

## Results and Discussion: Ras Dynamics

**Introduction:**

Ras proteins influence many different signaling cascades through their interaction with various effectors and modulators. However, individual Ras effectors are very different proteins although they share a common motif: the Ras Binding (RB) or Ras Association (RA) domain. RB encodes the specificity for Ras interaction within a few key residues in these domains [99]. The ability of Ras to associate with different effectors and modulators suggests that it adopts various conformational states, which have been well studied using X-ray and NMR. However, due to a preconceived notion that H-ras and K-ras were identical in their biological properties, much of the previous biological and biochemical assays were done on H-ras [45]. Recent studies described in Chapter 1 reveal that there are levels of specificity amongst Ras isoforms for different effectors and modulators. Moreover the specificity of the H-ras mutants Y40C and T35S to the effectors PI3K and Raf respectively suggests that this may be due to changes in the allosteric behavior of the proteins since neither of these residues are directly involved in association with either effector. Also studies have shown that K-ras and H-ras display a degree of specificity in activating the effectors Raf and PI3K, this was found to be not limited to their difference at the HVR and/or membrane localization [37]. Furthermore the occurrence of Ras genes in human cancers reveals that isoform specificity plays both a role in frequency of a particular isoform and the specific point mutation in various cancers [50]. Taken together the effector specificity of H-ras and K-ras towards the major effectors PI3K and Raf, coupled with the isoform specific frequency and

localization in specific cancers further highlights the need for a detailed analysis of the differential dynamics between these isoforms.

In order to study the specific dynamics of Ras isoforms or to understand the ability of Ras interaction with various effectors and modulators we must first consider the role of conformational selection in Ras function. The central postulate of conformational selection is that all protein conformations pre-exist and that the most favored conformation is selected by the ligand, resulting in a shift and a redistribution of conformational states following ligand binding. Subsequent to the population shift an induced fit mechanism may optimize side chain and backbone interactions [100]. In this Chapter I investigate the dynamics of Ras in distinct conformational states. Firstly I will compare the overall dynamics of H-ras and K-ras though PCA. Then the dynamics of specific conformational clusters of H-ras and K-ras (described in Chapter 3) is compared to those of T35 H-ras mutants. These MD conformers are then related to the conformations of the crystal structures of nucleotide bound Ras through PC projection. Lastly I analyze the conformational dynamics of the Q61H mutants. The selection and analysis of conformational clusters described here are a fundamental step in accessing the dynamics of Ras·GTP. All of the analysis in this Chapter is based on the backbone, which is represented by the C-α atoms details of the atomic interactions within each substate of each protein will be addressed in Chapter 5.

**4.1 Increased inter-lobe correlated motions in H-ras relative to K-ras.**

To investigate the overall dynamics of our systems we applied PCA to the entire trajectory of each system. The contribution of specific residues to the PC's differs significantly for H-ras and K-ras, especially at switch I and some loops on lobe II (Figure 4.1). The variance represented here is indicative of the dynamics where a high contribution to the PC represents

a very dynamic region. These dynamics captured by the first 3 PC's, which accounts for ~50% of the total variability of the data in our systems (see Figure 3.4), reveals that there are significant conformational differences between the two isoforms. Overall, K-ras is more flexible than H-ras at switch I whereas H-Ras is more dynamic at loop regions in lobe II.
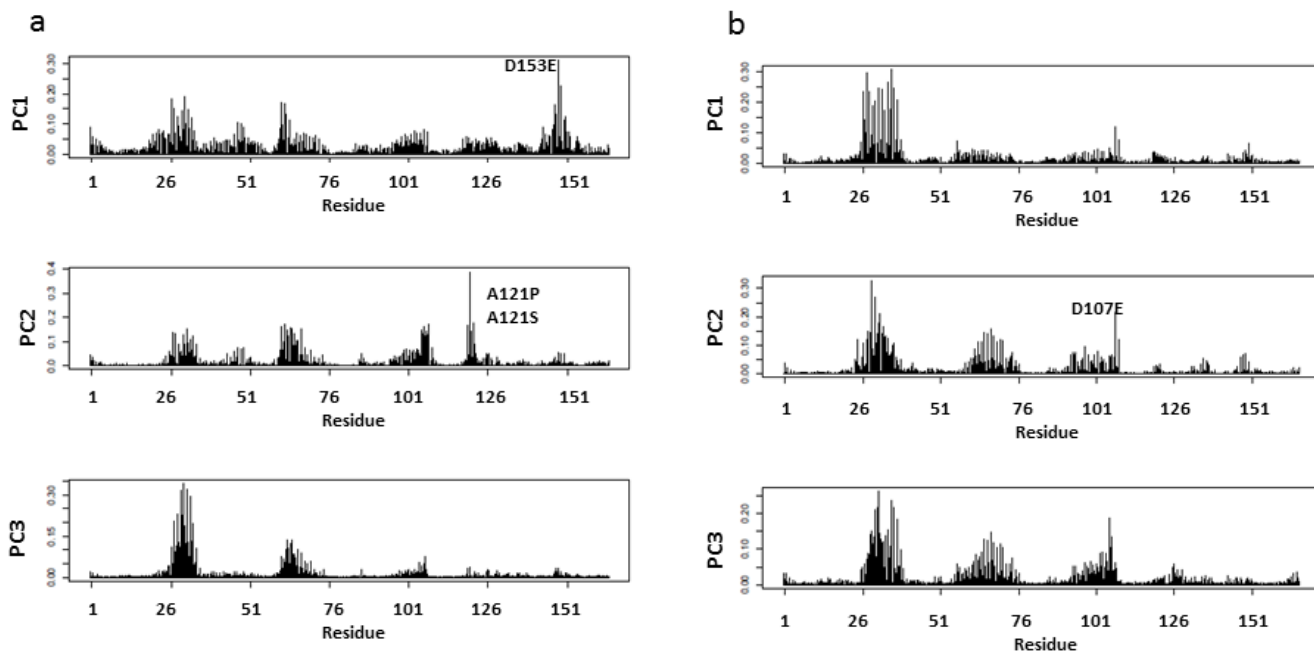


**Figure 4.1**: PCA loadings or contributions of each residue (Cα coordinates) to the variance over all conformations of H-ras(a) and K-ras(b).

| Region | Residue (approximate range) |
|---|---|
| Switch I | 25-40 |
| Switch II | 60-75 |
| L7 | 104-111 |
| L8 | 118-127 |
| L10 | 148-155 |

**Table 4.1:** Secondary structural element of Ras with corresponding residue numbers. These serve as a reference for different structural regions on Ras mentioned in this study.

DCCM analysis of the entire trajectory suggests that several transitions have occurred in H-ras, involving changes in loops at lobe II and increased correlated motion between lobes I and II. The increased dynamics at L8 and L10 of H-ras appears to be correlated with a series of regions across the entire protein. These coupled motions are greatly reduced in K-ras (Figure 4.2). The change in RMSD of L10 seems to be related to fluctuation in the switch I regions for both H-ras and K-ras (Figure 4.3 (a) and 4.5). Interestingly L10 RMSD for H-ras is almost twice that of K-ras and T35S. The plot of conformers colored by cluster clearly shows that the displacement of L10 involves major conformational change in H-ras. This may suggest a specific role for key residues on the loops of lobe II for differential dynamics between H-ras and K-ras.
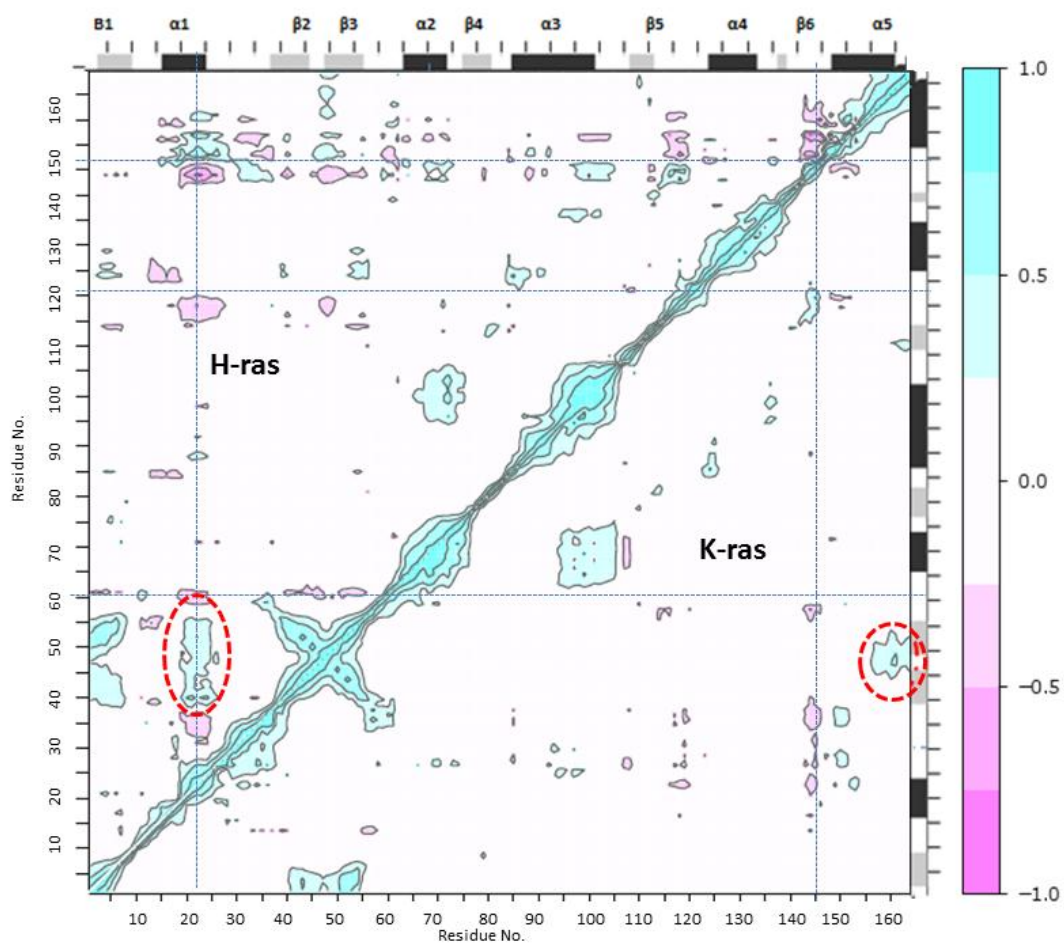
**Figure 4.2:** DCCM plots of H-ras (upper triangle) and K-ras (lower triangle) Cα atoms. Red circles highlight correlated motions previously described.
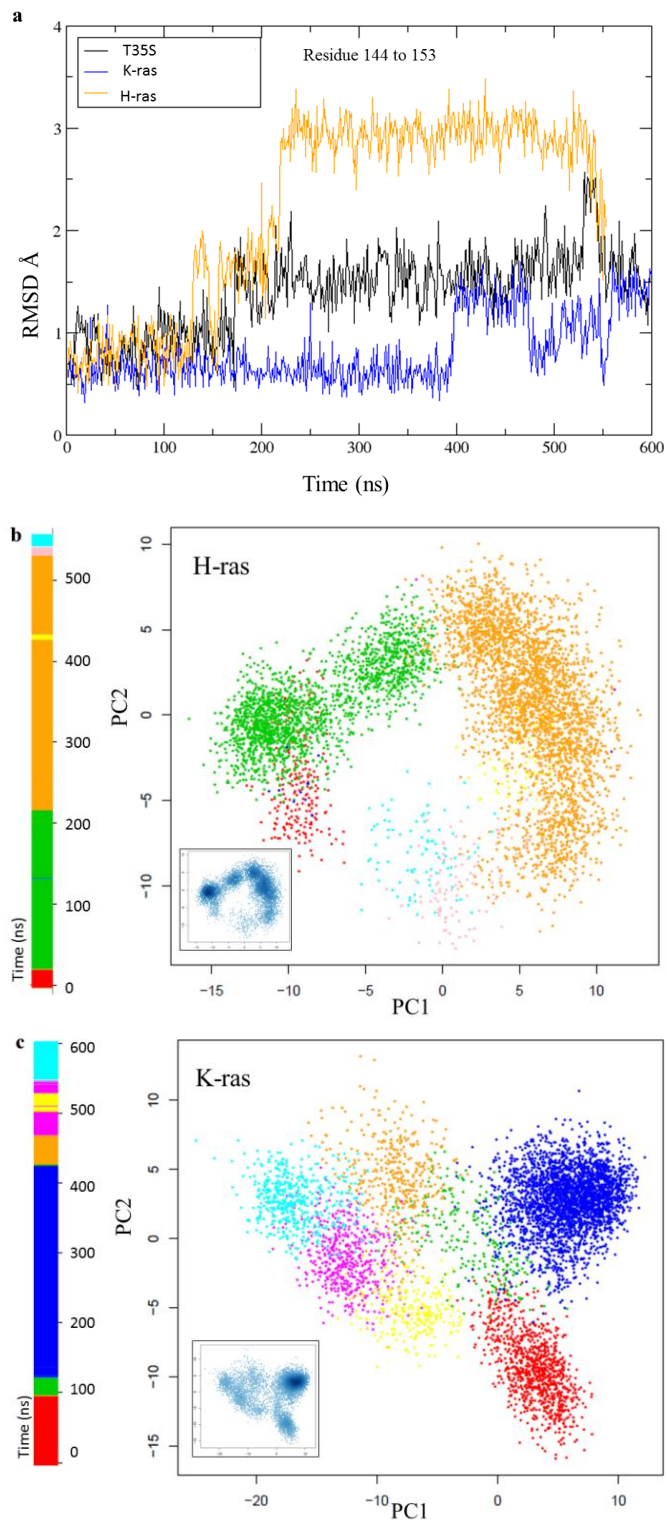
**Figure 4.3 :** Cα RMSD of residues 144-153 (a). PCA projection of conformers for H-ras (b) and K-ras (c) are colored according to their RMSD clusters. Inset shows PCA projections colored by density.

40

## 4.2. Comparison of state I/ State II populations of H-ras and K-ras

A distance plot (see section 3.3) was utilized to differentiate between states I and II as well as among intermediate states. We observe that K-ras is more dynamic than H-ras at switch I where there is a direct transition to a state I-like intermediate as T35 loses coordination with the $Mg^{2+}$ ion and switch I opens at T35 (Figure 4.4). This is consistent with NMR studies that report a slightly higher probability of K-ras to sample state I conformations [25,28]. The Y32-G12(Cα) plot suggests that this region of switch I is more flexible in K-ras and has a different conformation from H-ras. This is indeed the case as previously mentioned (see 4.2). Similarly, T35S H-ras adopts a more open switch I conformation than H-ras, with two distinct populations. However the S35-G12 (Cα) distance of cluster 1 (~150-300ns) correlates well with the crystal structure reported for T35S in a state I intermediate conformation termed state I /form II. [29]. The Y32-G12 (Cα) distance for T35S mutant is similar to H-ras WT, which is also characteristic of T35S state I/form II. In contrast the T35A mutant has a strong deviation at switch I, especially at residues 35 and 32, indicating an almost entirely state I population, in agreement with NMR data [26,28].
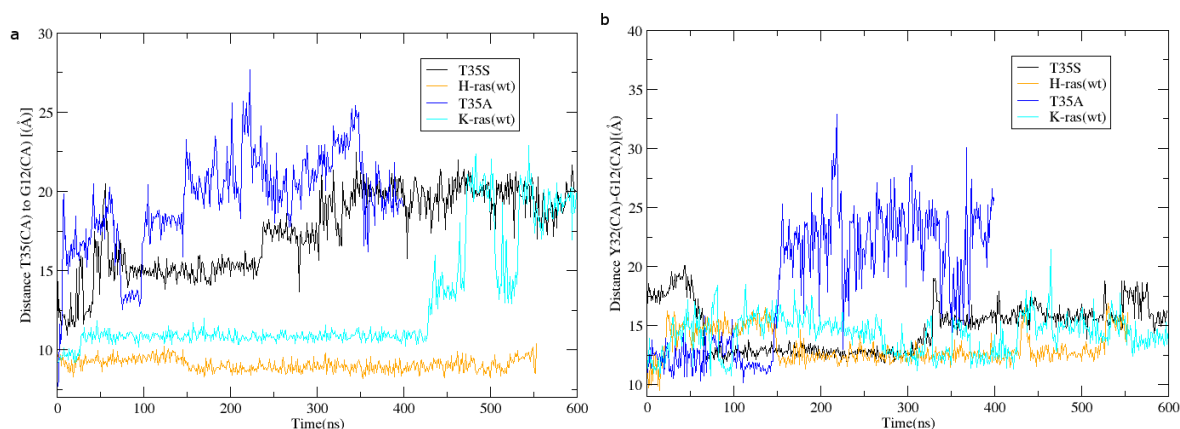


**Figure 4.4:** Distance between Cα atoms of residue T35 and G12 (a). Distance between Cα atoms of residue Y32 and G12 (b).

**4.3 Conformational clusters identified by the first few PCs highlight specific structural differences between conformers.**

To define specific conformational clusters, a dissimilarity matrix was prepared for hierarchical clustering using either the first 4 PC's or the pairwise RMSD of all Cα atoms. The PC derived clusters are representative of conformers that differ primarily due to the switch dynamics for K-ras and L10 dynamics for H-ras (Figure 4.5). However a comparison of RMSD derived clusters shows that it coincdes with the T35-G12(Cα) distance for the proteins (Figure 4.5). A comparison of the two methods clearly show that the PC method is more sensitive to conformational differences since these clusters are also dependent on switch II. We therefore concluded that PC based clustering provides a more refined method of clustering to discriminate between conformers[11]. However as previously desribed, plotting the T35-G12 Cα distance can be useful in categorizing state I/II intermediates, therefore we have used the RMSD clusters for further analysis of state II intermediates.

---

[11] For each system the same number of clusters was selected for both the PC and RMSD method.
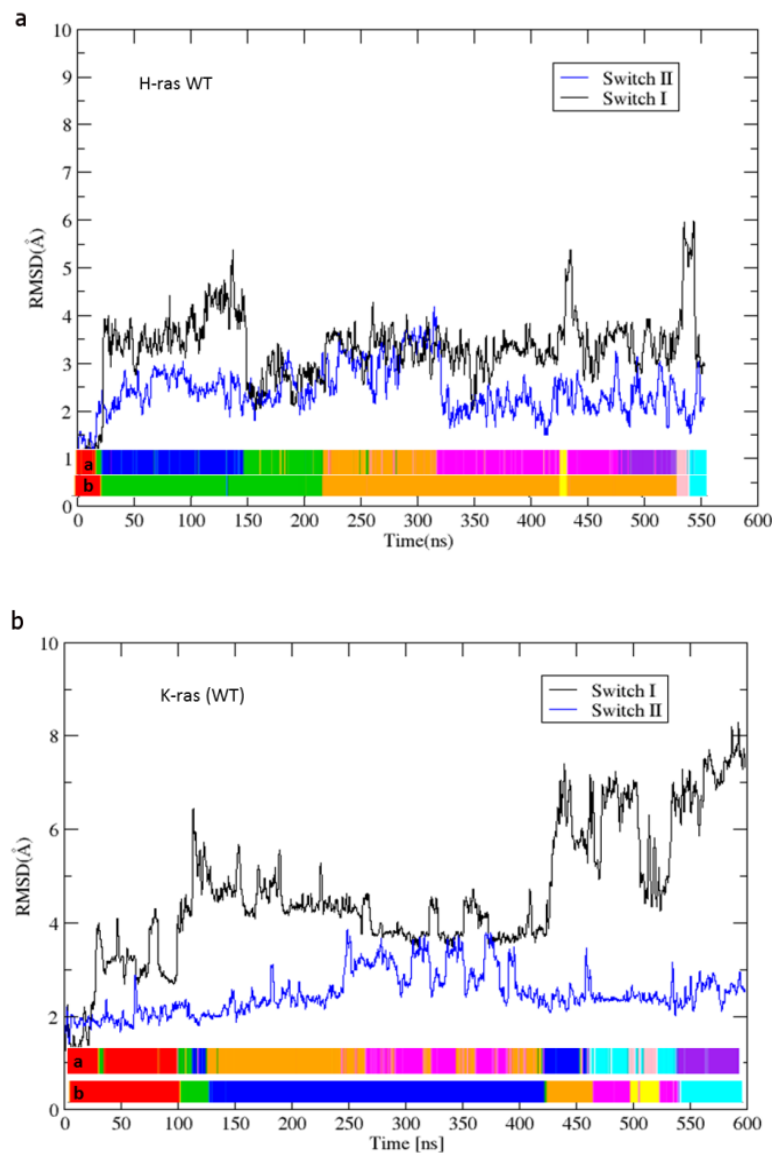
**Figure 4.5:** RMSD of Cα atoms of switch I (black) and switch II (blue) for H-ras (a) and K-ras (b). Colored bars represent different conformational clusters based on PC (top) and RMSD (below). Different colors represent different conformational clusters as defined by the PC or RMSD, however the colors are simply to highlight clusters and their magnitude accoridng to their sampling during the simulation.

**Projection of MD conformers reveals distinct conformational populations for Ras isoforms.**

In order to visualize MD conformers in relation to the crystal conformers we used a projection tool which utilizes the mean and the PCA loadings values from the crystal

43

conformer data set to calculate the variance. Hence these conformers can be projected onto the PC's defined by the crystal data set. Accordingly the conformations are represented based on their variance from the crystal structures according to the PCs. An initial inspection of the projected conformers reveals that the MD conformers are very dynamic and sample a large region of PC space along the first two principal components. Since switch I and II dictates most of the variance of the first few PCs amongst the X-ray structures, projection onto PC 1 and PC 2 essentially describes the conformers based on their similarity at the switch regions. The conformer plot of T35A H-ras clearly shows that it is very dynamic and samples a region of conformational space in terms of both PC 1 and PC 2. Furthermore there are distinct conformational clusters for the wild type isoforms. The difference is even more evident between the Q61H mutants of H- and K-ras. The T35S mutant and WT K-ras both have two distinct clusters, which are representative of the large deviation of switch I in both these systems.
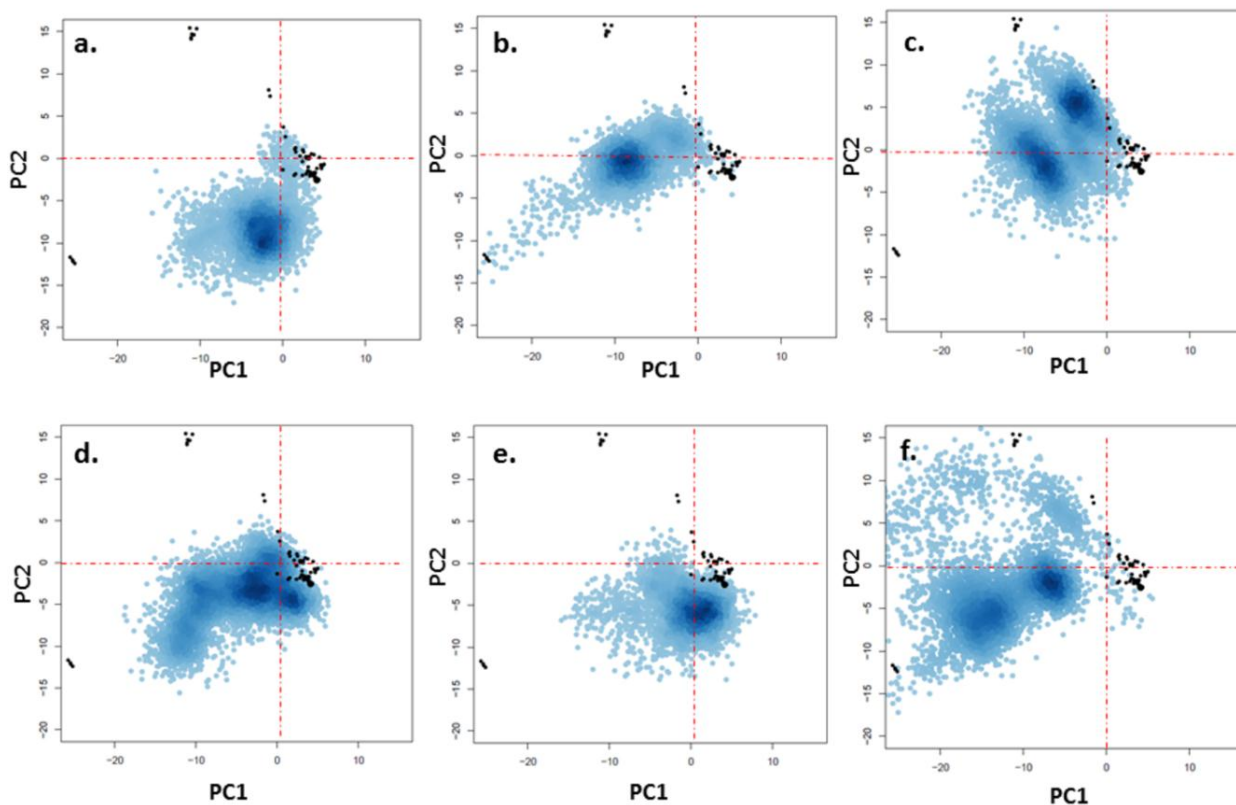
**Figure 4.6:** Distribution of Ras MD conformers in PC space with blue points representing MD conformers and lack dots crystal conformers. a-e; H-ras (wt), Q61H-H-ras, T35S-H-ras, K-ras (wt), Q61H-K-ras, T35A-H-ras.

**Analysis of conformational clusters reveals similar dynamics for K-ras and the T35S**

**mutant.**

Dynamic cross correlation analysis of the major K-ras and H-ras clusters show that there are

altered correlated motions between the two isoforms. A closer look at the residue correlations

(fig 4.7 (a)) reveals that more residues are involved in correlated motions between switch II

and III (1)[12] in K-ras than H-ras. Correlation is also observed between switch I and the α

helix of switch II (3). Lastly the correlation between the C-terminus and β2-L3-β3 (2) is

present throughout the K-ras simulation but is significantly reduced in H-ras. This may

indicate a communication pathway between lobes I and II that is always present in K-ras but

---

[12] These are labeled on Figure 4.5 for easy reference.

only appears during transitions in H-ras [59]. Furthermore we observe that  H-ras has comparable dynamics to previous results obtained from accelerated molecular dynamics simulations of H-ras.[59]. T35S H-ras displays correlated motions more comparable with K-ras. Correlations between switch I and II and between $\beta2$ and $\beta3$ are maintained in K-ras and T35S H-ras, however there is increased correlation between helices III and IV for T35S. Additionally correlation between residues 40 and 25 is not observed in T35S and K-ras but is present in H-ras and T35A. For T35A H-ras the correlation between $\alpha$ helices III and II is weakened, which is similar to the GDP state of H-ras [59]. Additionally there is anti-correlation between the P-loop and switch II, suggesting a possible role of these regions in the association with effectors.
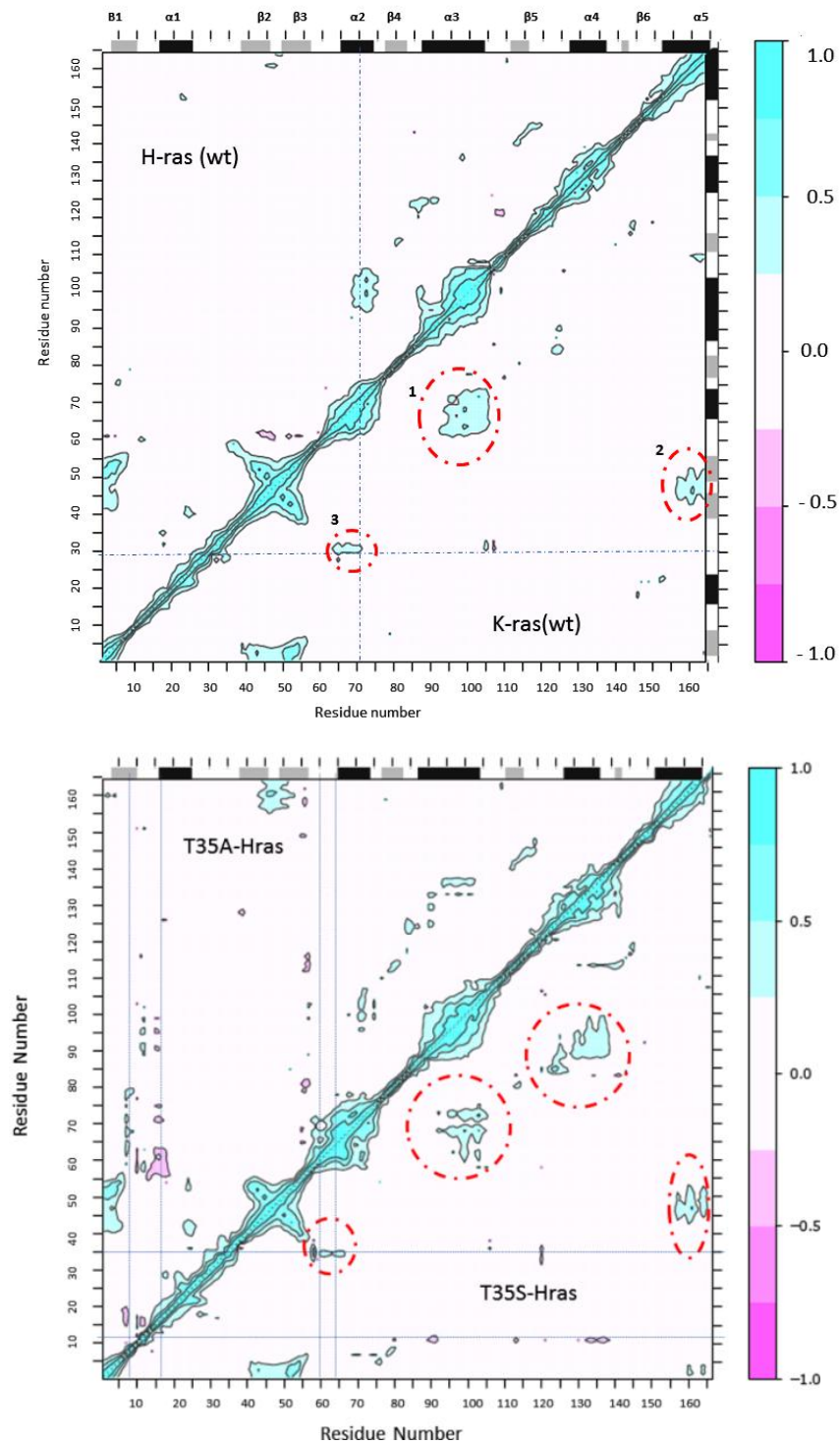
**Figure 4.7:** Dynamic cross correlation map of major RMSD clusters of H-ras (upper triangle) and K-ras (lower triangle) (top) and T35SA (upper triangle) and T35S (lower triangle (bottom).

To further investigate the dynamics that may affect the correlated motions within conformational clusters we looked at RMSF's of each system relative to H-ras. Figure 4.8 (a) shows the ΔRMSF for K-ras and T35S while Figure 4.8 (b) compares T35S to T35A. We observe that helix I of K-ras and T35S is more rigid but there are increased dynamics at the switch I loop. We also notice a decrease in the dynamics of switch II and also L8. Both K-ras and T35S are more dynamic at L10 and L7 particularly residue 107. However there is an increase in flexibility at helix III in T35S H-ras, which may account for the increased communication between α helices III and IV mentioned earlier. Additionally both K-ras and T35S have decreased dynamics at β2-L3-β3 (residues 40-50), which may account for correlations observed with the C-terminus that is absent in H-ras. The comparison of T35S to T35A reveals increased dynamics at the switches for T35A. Since the T35A mutant shares similar dynamics to H-ras at residues 107 and L8, which differ for T35S and K-ras, we certainly realize the implications of these specific residues in altering the conformational dynamics between isoforms, hence affecting effector interactions.
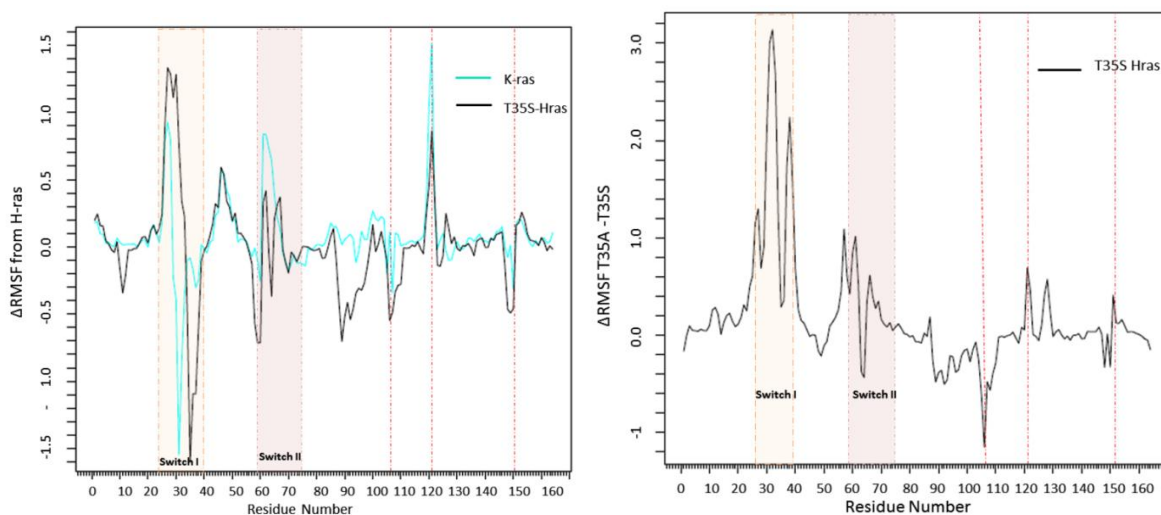


**Figure 4.8** RMSF difference plots between major cluster (ΔRMSF) from H-ras (top) T35A (bottom). Switch regions are highlighted and dotted red lines highlight residues in L7, L8 and L10.

## 4.4 Dynamics of Ras Q61H Mutants

To access the effects of specific mutations on Ras isoforms we studied the dynamics of the Q61H mutants of H-ras and K-ras, from here on Q61H-H and Q61H-K. There are distinct conformational populations for these mutants (Figure 4.5). Additionally cluster analysis reveals two conformational clusters of Q61H-H, which differ in the switch I region. In this case switch I opens at Q61H-H resulting in state I intermediate conformations (Figure 4.9). Conversely Q61H-K adopts a large conformational cluster, which is less flexible at switch II, and does not sample state I (Figure 4.10).
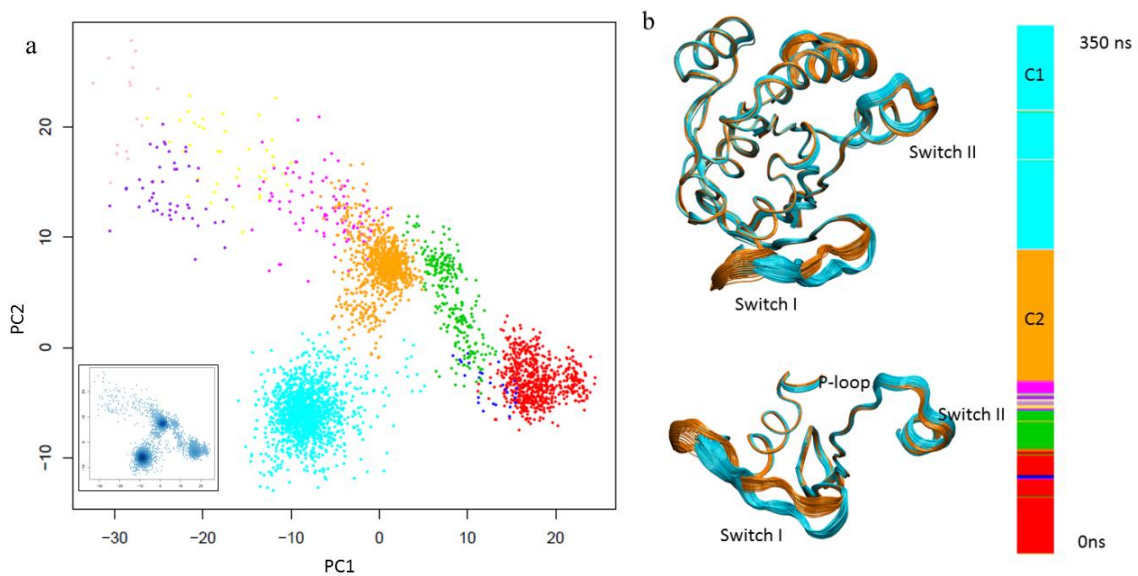


**Figure 4.9:** PC plot of Q61H –H-ras (a) Inset: density colored projection. Overlay of backbone conformations of the major clusters C1 and C2. (b)

49
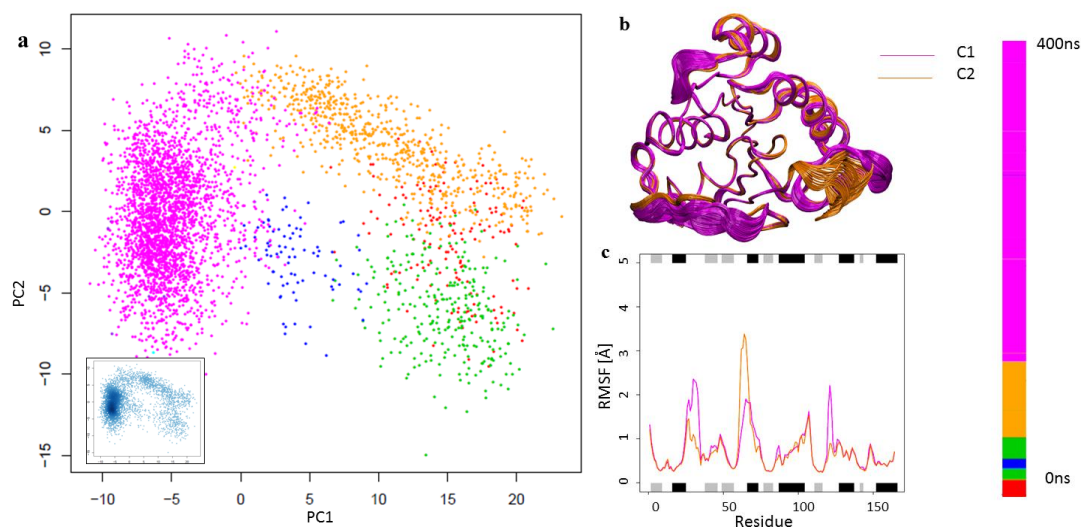
**Figure 4.10:** PC plot of Q61H –K (a) Inset; density colored projection. Overlay of backbone conformations of the major clusters C1 and C2. (b) RMSF of clusters 1 and 2 for Q61H K-ras.

For further analysis we describe the dynamics of the major clusters for the Q61H mutants.

Interestingly Q61H-K is more similar to H-ras in terms of correlated motions and dynamics.

Firstly DCCM analysis shows a correlated motion between residues 40 and 25 and also between helix III and L8 on Q61H-K but not Q61H-H (Figure 4.11). Q61H-H retains flexibility at L10 similar to H-ras, however Q61H-K has altered dynamics compared to K-ras. For example there is an increase in flexibility at L8 and decreased flexibility at L7. In comparison Q61H-K is more dynamic at switch II than Q61H-H, which samples State I-like conformations. This may provide critical clues into the isoform specific oncogenic potential of certain mutants; in particular Q61H-H may have oncogenic potential via rapid cycling through state I/II conformations. Meanwhile the same mutations may affect K-ras differently since increased dynamics of switch II may hinder its ability to associate with GAPs [18,101]. Additionally this may also affect the interaction with effectors and GEF's that interact with switch II, hence decreasing the oncogenic potential of Q61H-K. NMR studies on Ras mutants showed an increase in GAP hydrolysis upon selection of state II [25] and the Q61L

H-ras mutant is susceptible to GAP mediated GTP hydrolysis whereas the H-ras G12V mutant is not [102]. We therefore gain critical insights into the conformational dynamics of these mutant isoforms that may explain the difference in oncogenic potential observed for specific isoforms of Ras mutants.
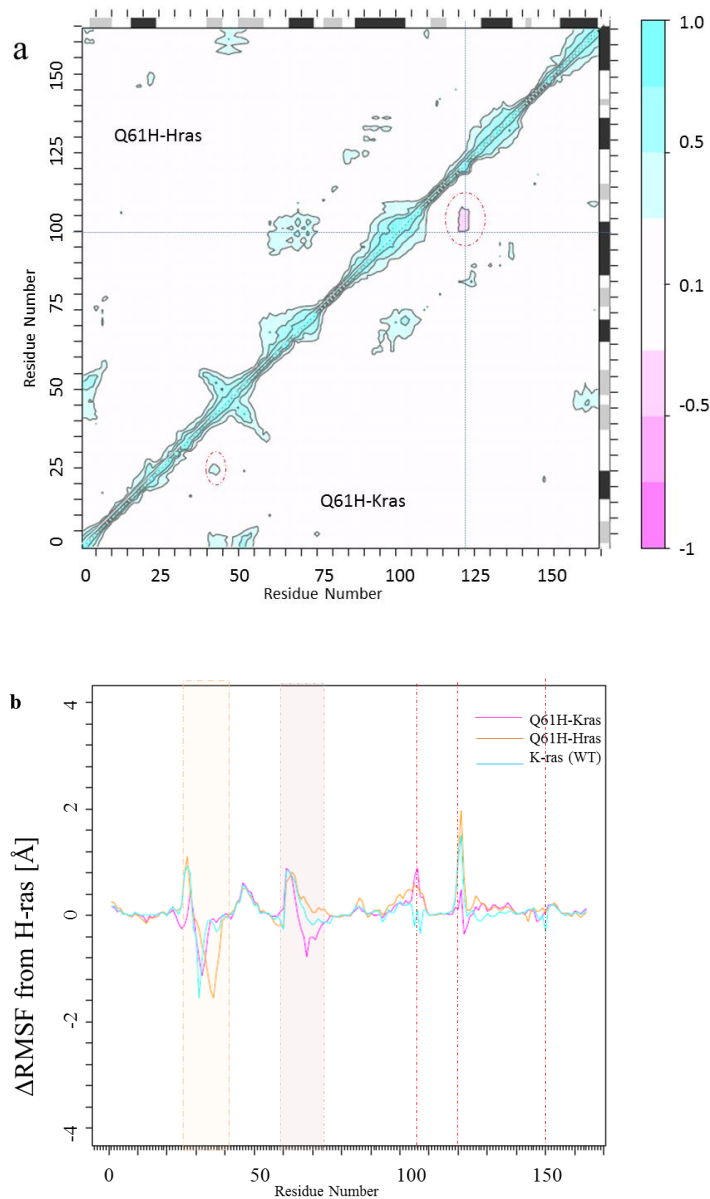


**Figure 4.11:** Dynamic cross correlational analysis over Q61H H-ras and K-ras mutants (a) RMSF difference plots between major cluster (Δ RMSF) from H-ras (b)

**Discussion**

Based on our conformational analysis of the protein backbone we have shown that K-ras and T35S H-ras mutants are similar in their dynamics and correlated motions. For T35S the increase in the dynamics of residues Y64 and D63, which are crucial for associating with PI3K [15], may partially explain the loss of specificity to PI3K since these residues are involved in the interaction of Ras with PI3K.

Mutations in the switch II region of Ras have been shown to perturb interactions with various effectors [103]. In our analysis of the backbone H-ras and K-ras display very different dynamics in the switch II region. On the other hand K-ras is more dynamic than H-ras at switch I, which may explain the preferential interaction of H-ras with Raf-RBD [46]. The stability of switch II in K-ras may be a factor in the preferential activation of Raf by K-ras, since switch II interaction with the cysteine rich domain of Raf is necessary for its activation [104,105]. Stabilization of switch II on K-ras may also affect its affinity for specific GEF's, effectors and calmodulin since switch II residues are involved in these interactions [48,106,107]. Additionally, previous molecular dynamics simulations on the Ras–Raf complex of H-ras showed a decrease in the dynamics of switch I/II, β1 and L7 regions upon complex formation [108].

**A role for increased dynamics on lobe II**

Another important observation is the reduced flexibility of L8 on K-ras in a similar manner to that of T35S H-ras. Loop 8 (residues 119-125) adjoins the amphipathic helix IV, which contacts the membrane. Decreased flexibility at this region may affect the membrane interactions. Usually the substitution of any residue for proline renders rigidity in the protein backbone since its side chain is part of the backbone [109]. Hence the A122P substitution on

K-ras could stabilize this loop and may contribute to the increased dynamics and transition to a state I intermediate of K-ras previously reported [25,94]. However we would like to note both K-ras and H-ras display enhanced dynamics at different regions. In particular, K-ras is more dynamic at switch I whereas H-ras is considerably more dynamic in lobe II. These differential motions in lobe II, specifically L10-Helix IV residues, are correlated with major conformational changes in the effector loop (switch I) of the systems studied. Consequently the dynamics of this region may also influence the orientation of Ras proteins on the membrane, since these residues are located towards the C-terminus and anchor of the protein. Overall we have determined that the correlation and flexibility between lobes I and II is very different for H and K-ras and affects the conformations of the effector binding loop more significantly in H-ras than K-ras.

**Specific mutations affect the conformational distribution between Ras isoforms**

Furthermore the Q61H point mutation alters the conformational distribution of K-ras and H-ras differently. The same mutation leads to state I intermediate conformations in H-ras but not K-ras. This could partially explain why somatic Q61 H-ras mutants are found more frequently in H-ras related cancers than in those of K-ras [50], and is consistent with NMR studies that have shown that mutants which have oncogenic potential and low GTPase activity tend to adopt state I like conformations [28].

To conclude we have shown that the substitution of various amino acids on lobe II of H-ras and K-ras results in differential dynamics between these proteins. Interestingly the T35S point mutation on H-ras results in conformers that more resemble K-ras. Lastly the Q61H point mutation results in distinct conformational populations. In this case the H-ras mutant sampled state I-like conformations while the K-ras mutant sampled state II.

The role of specific residue interactions that affect the conformational dynamics will be discussed in Chapter 5.

## CHAPTER 5

## The role of Specific Residue Interactions between Ras isoforms

**Overview**

X-ray crystallography and NMR studies of Ras in complex with various effectors and modulators have identified key elements on the effector binding loop and the switch II region that are necessary for the Ras-effector/modulator association[15,17,18,19,21,61]. Although, the RBDs of the Ras effectors Raf, PI3K and Ral have very little sequence homology they have substantial structural similarities in their RBD [110]. The specificity of Ras isoforms towards the effectors Raf and PI3K [37] suggests that the effector binding loop of Ras may achieve specificity through sampling various conformations. Therefore, different conformations may permit specific association with effector/modulator proteins through differences in the dynamics and through the rearrangements of specific residues. In Chapter 4 we have investigated the conformational dynamics within conformational sub-states of H-ras and K-ras isoforms and specific mutants. In this chapter we will explore the specific side chain contributions to the dynamics and overall conformation in terms of salt bridges, hydrogen bonds and hydrophobic contacts. First we will investigate the unique contacts in K-ras and H-ras and compare them to those in T35S H-ras (T35S). We then investigate the conformations of Q61H mutants to probe for specific contacts that may explain the differential conformational dynamics previously described between the H and K-ras isoforms of this mutant.

## 5.1 K-ras and T35S H-ras are similar in terms of their side chain interactions

We have utilized the contact map described in Chapter 2 to find contacts that are unique for each conformational cluster of our system. First contacts were determined for each system in

terms of occupancy (% contacts) within the conformational cluster and then subtracted from those made in H-ras. Only contacts that were unique and had at least 50 % occupancy were considered for analysis. An inspection of the global contacts unique for K-ras and T35S reveals that they share similarities in the residue interaction profile (Figure 5.1). The T35S simulation was started from the crystal structure (3KKN) [98] in a state I conformation and it sampled a wide region of conformational space, however we have selected a cluster reminiscent of state I form II for analysis. The similarity of this mutant in terms of conformational dynamics to K-ras is quite striking, considering that T35S is a point mutation on switch II, whereas K-ras differs from H-ras in terms of several residues on lobe II.
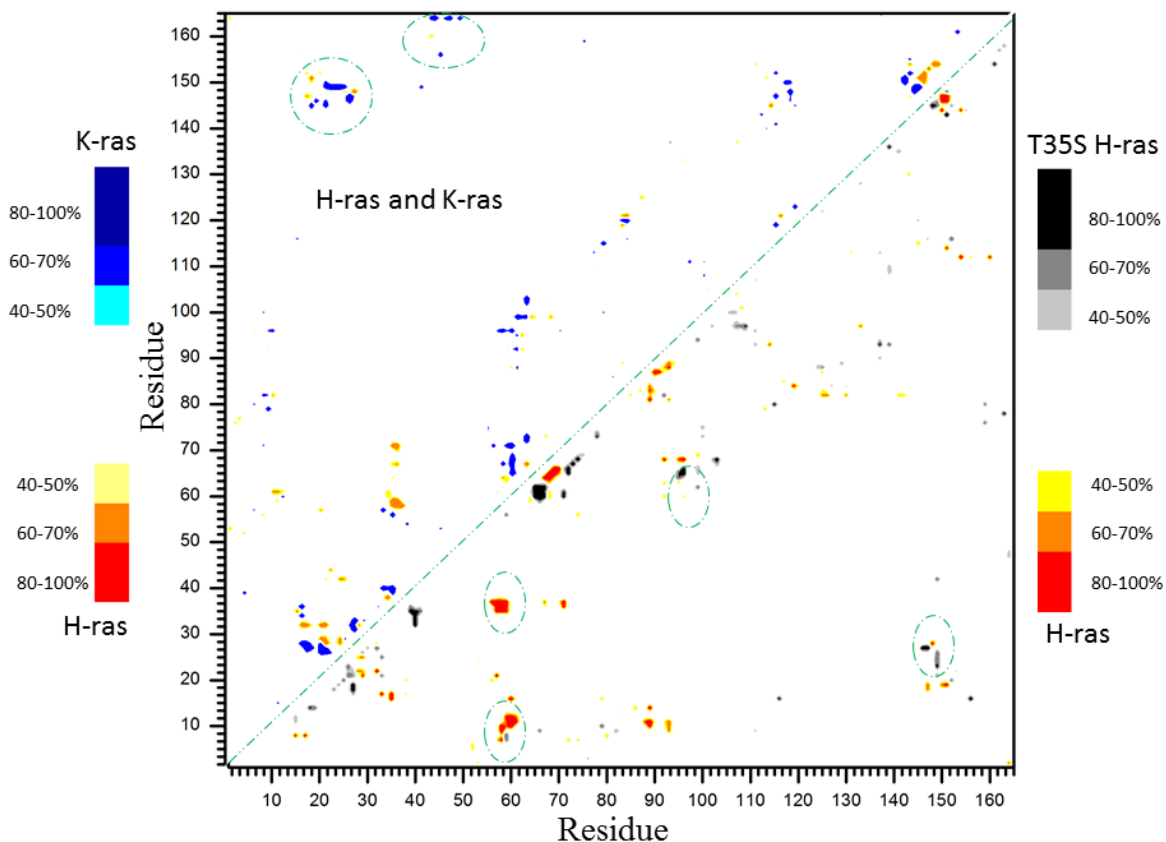
**Figure 5.1:** Time averaged residue contacts in H-ras, K-ras and T35S-Hras clusters. Color Bars represent the occupancy of the contact and unique contacts for either K-ras vs H-ras (upper triangle) or (T35S vs H-ras). H-ras specific contacts are colored yellow to red, K-ras cyan to blue and T35S grey to black. A contact is described as any two side chain residues within 4Å of each other.

## Absence of Y71–E37 and E37-A59 H-bonds in T35S-H-ras and K-ras may explain their similar dynamics

There are frequent contacts between switches I and II that appear to be unique for H-ras (Figure 5.1). This is actually due to the presence of a H-bond between the Y71 OH and the acidic oxygen on E37 that is almost absent in K-ras and T35S. This contact is replaced by a H-bond between A59 N and Y71OH on K-ras and T35S (fig 5.2). The replacement of a threonine with serine disrupts the hydrogen bonds between the I36 O and A59 N in T35S H-

57

ras, which also affects the E37-Y71 H-bond. Interestingly the I36-A59 H-bond is also broken in K-ras. Since residues I36 and E37 have been shown to interact with both PI3K and Raf [15,20], differential contacts in this region may result in different preference for effectors.
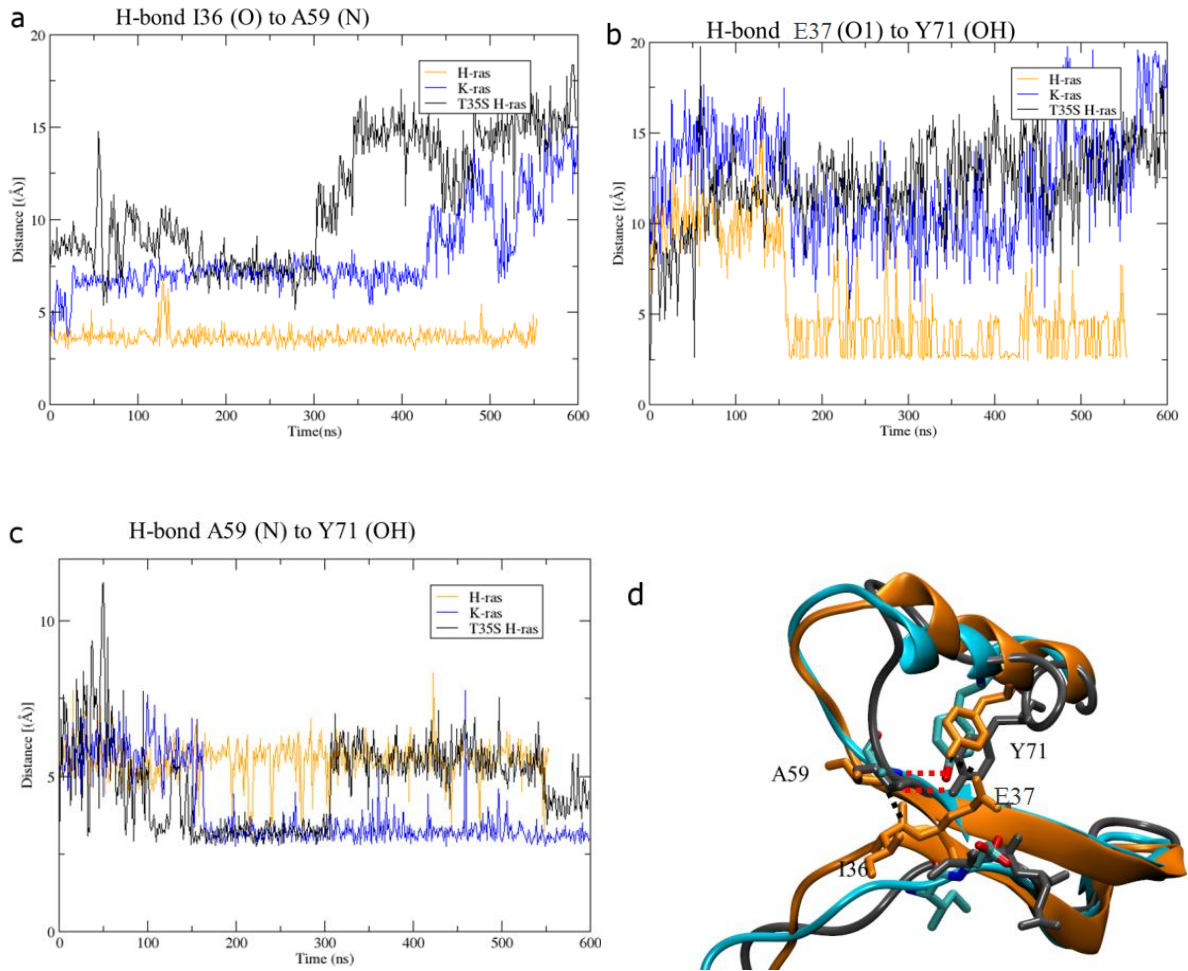


**Figure 5. 2:** Hydrogen bonds represented by distance between the donor and acceptor atoms for H-ras(orange), T35S(grey) and K-ras(blue). (a) I36-A59 H-bond, (b) E37-Y71 H-bond, (c) A59-Y71 H bond (d) H-bonds unique to H-ras are represented by black dotted lines and for K-ras and T35S red dotted lines.

**Switch I residues D38 and E37**

There is an increase in distance between residues D38 and D33 in K-ras and T35S due to reorientation of the side chain of D38 (Figure 5.4). This may be due to above mentioned rearrangement of H-bonds between residues 37 and 71. The reorientation of residue 38 may also play a role in altering the negatively charged groove formed by D33-D38, which is important for favorable interaction with a lysine on the α helix 1 of effectors and β2 of NORE1 [107]. Another putative role of the reorientation of residue 38 is the specificity of the association with PI3K since the D38E mutant retains its ability to associate with Raf and not PI3K while the E37G mutant will only associate with Ral-GDS [47]. The reorientation of residue 38 in K-ras and T35S coupled with the sensitivity of the D38E mutant to PI3K and E37G to RalGDS suggests that these residues may play a role in fine tuning the Ras affinity for specific effectors. Furthermore, since NORE1 interacts with switch I through a lysine on its β2 strand, instead of α helix 1 present in other effectors, this interaction may be more favorable for K-ras where D38 is oriented outwards. We also observe different orientations of effector binding residues Q25 and N26 which are involved in hydrogen bonds in the Raf-Rap complex [61] .

**Specific switch II contacts: a role for Y64**

In K-ras we observe a reorientation of Y64 as it forms a stable hydrogen bond with D69 (Figure 5.3). Residue 64 plays a crucial role in interaction with effectors where it associates with a phenylalanine on the β1 strand of NORE1 [107]. In addition Y64 and Y71 form contacts with SOS [17]. The reorientation of this Y71 and its H-bond with D69 may therefore alter the preference of Ras for these effectors. This can in part explain the reduced affinity of K-ras to PI3K and SOS. Since the G12V/Y64G mutant is Raf-specific we may presume that

Y64 may be dispensable for Raf activation. However the Y64W mutation abolishes binding to the Raf CRD [105], thus there may be a specific role for the orientation of this residue since the bulky side chain and lack of an OH in Tryptophan may hinder interactions with Raf-CRD.
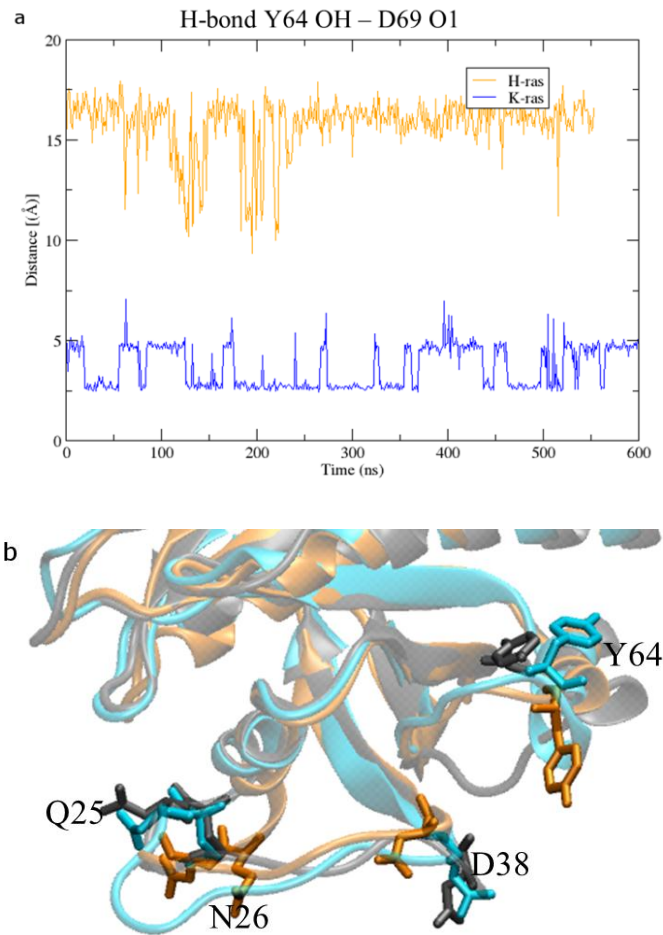


**Figure 5.3** H-bond between Y64 OH and D69 O (a). Orientation of specific residues on H-ras (orange), K-ras (blue) and T35S (grey) (b)

**A D119-K147 salt bridge stabilizes L8 and L10 in K-ras and T35S**

Residues 116-119 and 145-147 are part of the consensus guanine nucleotide base binding site on GTPases [111]. Interestingly monoubiquitination of K-ras at residue 147 increases its

GTP loading and enhances the affinity of K-ras G12V to PI3K and Raf but does not affect its localization in the membrane[112]. Ras isoforms have different ubiquitination sites: 104 and 147 on K-ras and 117, 147 and 170 on H-ras [112]. The two major ubiquitination sites are K117 and K147 on loops 8 and 10 respectively [112]. A salt bridge is formed between K147 and D119 (Illustrated in Figure 5.4 (d)). This contact is more frequent in K-ras and T35S (see Figure 5.1) which may account for the reduced flexibility of at L8. Previous molecular dynamics studies on the ubiquitination of proteins have proposed that the role of ubiquination is more of conformational restriction [113], hence we may speculate that ubiquination of K147 may alter the dynamics of K-ras via affecting the D119-K147 salt bridge to select conformations more favorable for effector interactions with PI3K.

**Specific roles of other residue contacts**

An decrease in contacts between the P-loop and switch II in T35S is due to the loss of the G12 N and G60 O H-bond. The G60A mutation moderately decreases the binding of H-ras to Raf RBD while significantly reducing the binding to RalGDS [114]. Likewise the T35S mutant also has decreased affinity to RalGDS [47], which specifies an involvement of the G60-G12 H-bond in stabilizing Ras conformations that associate with specific effectors. Residue 27, which also interacts with Raf (Figure 5.4 (b)), adopts a conformation towards the guanine base of GTP and the P-loop in K-ras. The crystal structures of H-ras·GTP and H-ras·GDP (pdb id 1QRA and 4Q21) clearly show that H27 adopts a different orientation with respect to the guanine nucleotide and K147 in the GTP and GDP state. The reorientation of H27 between H-ras GTP and H-ras GDP conformations, suggests that in H-ras this residue may play a role in conformational sensitivity to the nucleotide , which may in part affect the orientation of H-ras in the membrane due to the presence of GTP or GDP. However, since in

K-ras and T35S H-ras the orientation of H27 resembles H-ras GDP, the conformational sensitivity and ability to affect membrane orientation may be reduced or absent.
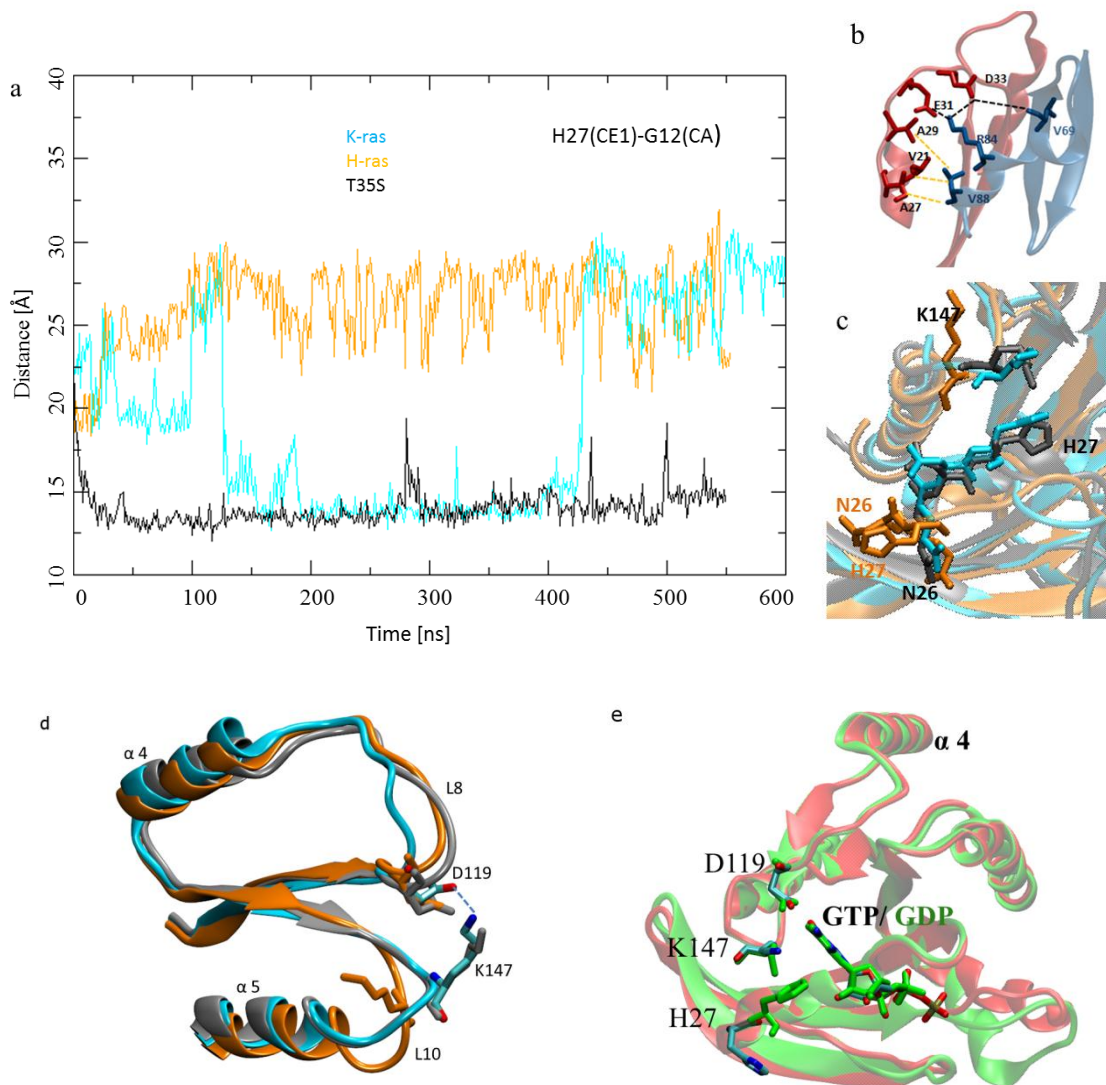


**Figure 5.4 (a)** Distance of H27 CE1-G12 CA in Hras (orange), K-ras(blue) and T35S(black). (b) Residue specific contacts of Rap-Raf complex with Rap in red and Raf in blue. (c) Side chain reorientation of H27, K147 and N26. (d) Salt bridge between K147 and D119 on K-ras and T35S crystal structures of H-ras·GTP (red) and H-ras·GDP (green) showing orientation of H27 with respect to K147 and the nucleotide.

## 5.2 Residue interactions in K-ras Q61H are similar to WT H-ras.

Previously we noted that the Q61H mutation perturbs the conformational equilibrium differently for H-ras and K-ras. Here we compared the overall dynamics of the WT isoforms

to the Q61H mutants. Q61H K-ras has a similar residue contact profile to WT H-ras (Figure 5.5). Firstly the H-bond between residue Y71 and E37 and G60- G12 is maintained in the Q61H K-ras mutant but not the H-ras mutant. The loss of these contacts appears to be coupled with the gain of the A59- Y71 H-bond on Q61H H-ras. Furthermore a unique salt bridge is formed between residues on helix III and II on Q61H-Hras (Figure 5.6). Since mutations at position 61 in H-ras are more frequently found in cancers compared to K-ras[50], one may reason that this mutation is more oncogenic in H-ras. In addition the similar contacts with T35S and WT K-ras suggest that it may potentially activate Raf better than Q61H K-ras. However, there is no current literature on the potential of these mutant isoforms to activate Raf. Although Q61H H-ras more readily adopts state I-like conformations in comparison to Q61H K-ras (Figure 5.6 (b)), oncogenic potential may also be achieved by rapidly cycling between state I and state II.
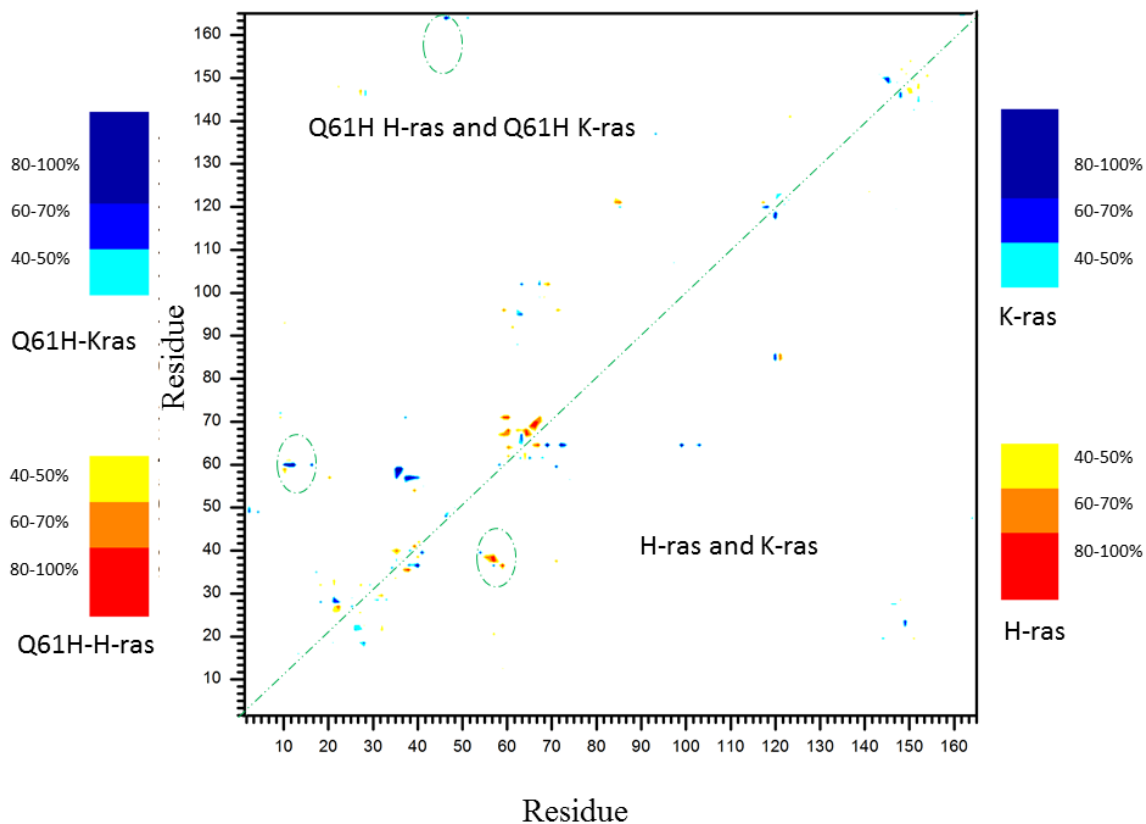
**Figure 5.5:** Time averaged residue contacts Q61H-Hras and Q61H K-ras simulations. Q61H K-ras contacts are subtracted from Q61H H-ras (upper triangle) and K-ras from H-ras (lower triangle). Contacts unique to H-ras/Q61H H-ras are colored yellow to orange based on occupancy and cyan to blue for K-ras/Q61H K-ras. A contact is described as any two side chain residues within 4Å of each other.
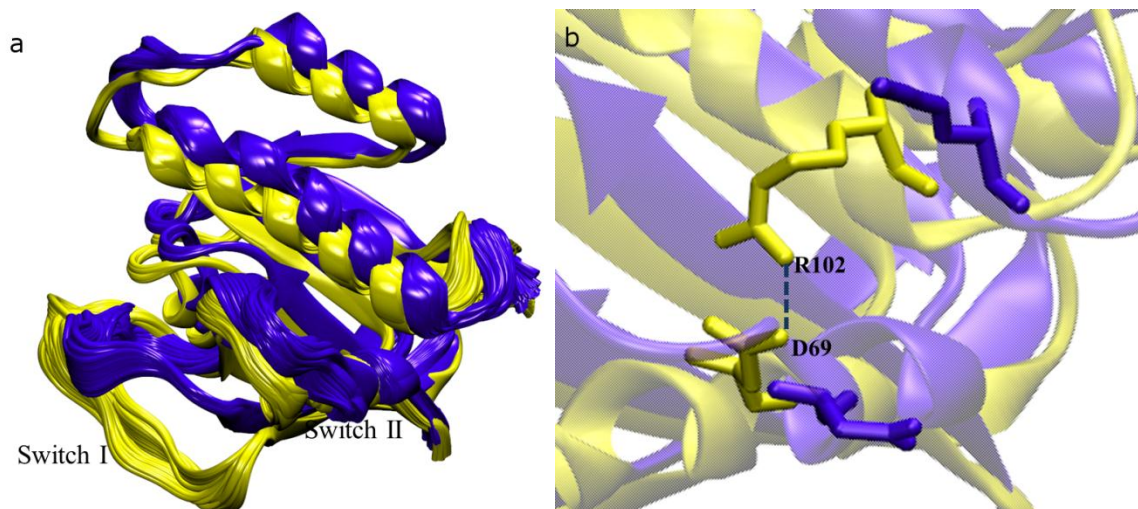
**Figure 5.6:** Secondary structure of Q61H H-ras and K-ras conformers (blue and yellow) respectively (a). Salt bridge between R102 and D69.

**Stabilization of the switch II helix in K-ras**

From our simulations, we mutated residue H61 on the Q61H mutant back to the WT. This change resulted in very different conformations of K-ras and the Q61H K-ras mutant. Interestingly it appears that the H61 may affect the switch II architecture in K-ras, by affecting the Y64-D69 H- bond. Furthermore we also note that the switch II helix forms an alpha helix in the wild type and a pi helix on the Q61H mutant K-ras.
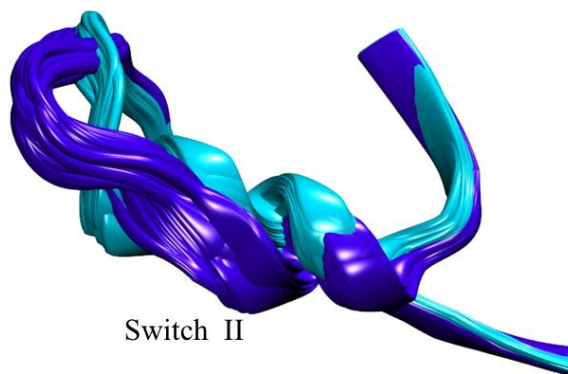


**Figure 5.7:** Switch II K-ras (cyan) and Q61H K-ras (blue)

65

**Discussion:**

In the previous chapter we have observed that in our simulations the T35S H-ras mutation results in a population of conformational sub-states that are similar to K-ras in dynamics; however the aim of this chapter was to investigate the conformation in terms of their residue contacts and side chain reorientations, which may affect or be affected by differential dynamics. We observe that T35S H-ras also has residue contacts that are similar to K-ras. To reiterate the loss of an H-bond on switch I residues I36 and A59 as well as on E37 and Y71 results in a A59-Y71 H-bond which propagates across the structure and results in conformations that are more similar to K-ras. These structural and residue rearrangements on T35S and K-ras that differ from WT H-ras suggest that they are involved in conferring a degree of conformational specificity for either favorable association with Raf or reduced affinity for PI3K. Furthermore the specific differences in residue contacts and orientations between Kras and H-ras at the switch regions, especially switch II, may influence effector specificity. Our primary reason for this assertion is because most effectors and modulators that have specificity for a particular Ras isoform, i.e NORE1, SOS, Ras-GRF, PI3K and Raf CRD and calmodulin, interact with the switch II of Ras [17,48,105,106,107]. Furthermore we have seen that the Q61H mutation drastically affects the conformational population towards state I on H-ras similar to the T35S substitution whereas the Q61H K-ras mutant more resembles H-ras WT in terms of dynamics and residue interactions. The differential effect of the mutation at position 61 may partially explain the prevalence of Hras Q61 mutant in cancers compared to mutants of Q61 K-ras mutants.

# Summary and Outlook

## Summary

There has been overwhelming evidence which shows Ras isoforms have non-redundant roles in the cell (reviewed in [45]). The aim of this study was to characterize the catalytic domain of H-ras and K-ras in terms of dynamics. We have shown that H-ras and K-ras differ in dynamics when bound to GTP and $Mg^{2+}$. The isoforms differ in flexibility at regions where there is sequence variation in lobe II as well as in the conserved, functionally important switch regions in lobe I.

This analysis has provided insights into a possible role of the H-ras and K-ras catalytic domain in their ability to recognize effectors in a specific manner. Our molecular dynamics simulations have resulted in two very distinct populations of H-ras and K-ras conformers that differ both in dynamics and conformation. In addition the simulations shows that K-ras is more dynamic than H-ras and has a higher tendency to a adopt state I populations within the time frame of the simulations. Moreover, conformer analysis revealed that the Raf-selective T35S H-ras mutant shares similarity with K-ras in terms of both dynamics and the side chain orientation of key effector/modulator binding residues at the switch regions. For instance, the switch I region of T35S H-ras resembles K-ras rather than H-ras. The conformational similarity between this mutant and K-ras provided us with a new view of dynamics that may enhance Raf activation, whereas the comparison between K-ras and H-ras provided new insights into some of the crucial elements for selective PI3K associations. Our data suggest that although H-ras has a higher affinity for Raf [46], which contacts Raf at the effector binding switch I [20], the switch II region of K-ras is so different in dynamics and side chain

orientations it partially explains the ability of K-ras to better activate Raf, since effective Raf activation involves the interaction of the switch II of Ras with the CRD of Raf [105]. We therefore conclude that H-ras and K-ras adopt different conformational populations and that K-ras fluctuates around a conformation that is more favorable for Raf association and not PI3K.

The implications of the variations in dynamics may be extended to differential orientation of the catalytic domain on the membrane surface since there is considerable flexibility in L8 of H-ras which adjoins the amphipathic α helix 4, which associates with membrane [115]. This is critical since studies have also shown that the nature of the bound nucleotide affects the membrane orientation of H-ras [115,116]. The relative rigidity of K-ras at L8 can potentially hinder its ability to reorient in the membrane. Furthermore, increased correlated motions between lobes II and I in H-ras may suggest that there is increased communication across the lobes so that lobe II of H-ras may be more sensitive to the nature of the bound nucleotide.

Furthermore specific Ras mutations alter the conformational distribution of H-ras and K-ras, with the Q61H mutation in H-ras but not K-ras resulting in state I-like sub states. This is an interesting finding since genomic studies have shown that the specific point mutation of Q61 appears to be both cell and isoform specific, with the H-ras mutations appearing to have a higher occurrence in tumors than those of K-ras [50]. This could be due to rapid cycling between state I and state II since state I Ras has low affinity for GAPs and high affinity for GEFs, resulting in faster nucleotide exchange [102]. Therefore the rapid cycling could result in a partially constitutively active protein with an oncogenic potential.

**Implications of the work for translational studies**

This work provides crucial structural information for isoform selective drug design to disrupt aberrant Ras signaling. Biochemical studies have shown that Ras mutants may alter the preference of Ras isoforms for different effectors and perturb the conformational equilibra between states I and II [25,26,28]. Additionally the occurrence of point mutations on Ras isoforms is variable and varies in frequency amongst different cancers and developmental diseases [24,50,102]. These results highlight the need to reassess the specificities of aberrant Ras signaling due to specific point mutations across isoforms. As we can clearly see we have identified distinct conformations of H-ras and K-ras and their Q61H mutants. The conformational analysis presented here highlights the usefulness of molecular dynamics to assess multiple conformations of the catalytic for drug discovery. Due to the high structural similarity among Ras GTPases, it has often been thought that targeting the catalytic domain may lead to many off target effects. Our results indicate that there are specific features between Ras isoforms, highlighting the need to study the dynamics of other members of the Ras family for targeted drug design. We propose that using molecular dynamics to access conformational sub states in members of a protein family can yield conformational ensembles and transient structures not revealed by other methods. Combining molecular dynamics with PCA can provide a manageable set of conformers and defined conformational clusters for docking.

**Further studies**: **Enhanced conformational Sampling**

A limitation of classical molecular dynamics simulation is the inability to sample all accessible conformations. To further determine the conformational sub-states not revealed by

our simulations, an enhanced sampling method such as accelerated molecular dynamics (aMD) may be used. Furthermore, utilization of the molecular mechanics/generalized Born surface area (MM-GBSA) methods [117,118] or thermodynamic integration [119]  may be useful to characterize energetic barriers between conformations.  Another area of interest is the dynamics of Ras-Raf complexes made by different Ras isoforms. Much analysis has been carried out on the structural dynamics of the Ras- Raf complex but these were limited to H-ras. The difference in dynamics we observed between H-ras and K-ras suggests that these data are not sufficient to explain K-ras/effector interactions. Hence, a further application of this work lies in addressing the conformational specificities and dynamics of isoform specific effector interactions. Finally, we mentioned above the possible effect of differential dynamics in the membrane orientation of nucleotide bound Ras. A comparative all-atom molecular dynamics simulations of membrane bound full length H-ras[115] and K-ras in both the GTP and GDP forms would be interesting.

In closing we have accessed the contributions of specific residue differences on lobe II of K-ras and H-ras and have discovered key differences in dynamics that alter the conformations at the functionally important switch regions. These differential dynamics may also alter the conformational properties of membrane bound Ras. This work shows that a general reassessment of Ras isoforms needs to be made since sequence differences may have a significant impact on conformational dynamics.

# BIBOLOGRAPHY

[1] M. Malumbres, M. Barbacid, RAS oncogenes: the first 30 years, Nature Reviews Cancer 3 (2003) 459-465.

[2] J. Harvey, An unidentified virus which causes the rapid production of tumours in mice, (1964).

[3] A.A. Adjei, Blocking oncogenic Ras signaling for cancer therapy, Journal of the National Cancer Institute 93 (2001) 1062-1074.

[4] J. Downward, Targeting RAS signalling pathways in cancer therapy, Nature Reviews Cancer 3 (2003) 11-22.

[5] V. Biou, J. Cherfils, Structural principles for the multispecificity of small GTP-binding proteins, Biochemistry 43 (2004) 6833-6840.

[6] K. Wennerberg, K.L. Rossman, C.J. Der, The Ras superfamily at a glance, Journal of cell science 118 (2005) 843-846.

[7] A. Rebollo, C. Martínez-A, Ras proteins: recent advances and new functions, Blood 94 (1999) 2971-2980.

[8] M. Trahey, F. McCormick, A cytoplasmic protein stimulates normal N-ras p21 GTPase, but does not affect oncogenic mutants, Science 238 (1987) 542-545.

[9] J. de Rooij, J.L. Bos, Minimal Ras-binding domain of Raf1 can be used as an activation-specific probe for Ras, Oncogene 14 (1997) 623.

[10] A. Wolfman, I.G. Macara, A cytosolic protein catalyzes the release of GDP from p21ras, Science (New York, NY) 248 (1990) 67.

[11] T.E. Dever, M.J. Glynias, W.C. Merrick, GTP-binding domain: three consensus sequence elements with distinct spacing, Proceedings of the National Academy of Sciences 84 (1987) 1814-1818.

[12] E. Santos, A.R. Nebreda, Structural and functional properties of ras proteins, The FASEB Journal 3 (1989) 2151-2163.

[13] J.F. Hancock, Ras proteins: different signals from different locations, Nature Reviews Molecular Cell Biology 4 (2003) 373-385.

[14] B.M. Willumsen, A. Christensen, N.L. Hubbert, A.G. Papageorge, D.R. Lowy, The p21 ras C-terminus is required for transformation and membrane association,  (1984).

[15] M.E. Pacold, S. Suire, O. Perisic, S. Lara-Gonzalez, C.T. Davis, E.H. Walker, P.T. Hawkins, L. Stephens, J.F. Eccleston, R.L. Williams, Crystal structure and functional analysis of Ras binding to its effector phosphoinositide 3-kinase $\gamma$, Cell 103 (2000) 931-944.

[16] C. Herrmann, Ras–effector interactions: after one decade, Current opinion in structural biology 13 (2003) 122-129.

[17] P.A. Boriack-Sjodin, S.M. Margarit, D. Bar-Sagi, J. Kuriyan, The structural basis of the activation of Ras by Sos, Nature 394 (1998) 337-343.

[18] K. Scheffzek, M.R. Ahmadian, W. Kabsch, L. Wiesmüller, A. Lautwein, F. Schmitz, A. Wittinghofer, The Ras-RasGAP complex: structural basis for GTPase activation and its loss in oncogenic Ras mutants, Science 277 (1997) 333-339.

[19] M. Geyer, C. Herrmann, S. Wohlgemuth, A. Wittinghofer, H.R. Kalbitzer, Structure of the Ras-binding domain of RalGEF and implications for Ras binding and signalling, Nature Structural & Molecular Biology 4 (1997) 694-699.

[20] S.R. Sprang, How Ras works: structure of a Rap–Raf complex, Structure 3 (1995) 641-643.

[21] N. Nassar, G. Horn, C. Herrmann, C. Block, R. Janknecht, A. Wittinghofer, Ras/Rap effector specificity determined by charge reversal, Nature Structural & Molecular Biology 3 (1996) 723-729.

[22] F. Wittinghofer, Three-dimensional structure of p21H-ras and its implications, Cancer Biol 3 (1992) 189-198.

[23] S.R. Sprang, G protein mechanisms: insights from structural analysis, Annual review of biochemistry 66 (1997) 639-678.

[24] A. Fernández-Medarde, E. Santos, Ras in cancer and developmental diseases, Genes & cancer 2 (2011) 344-358.

[25] M. Geyer, T. Schweins, C. Herrmann, T. Prisner, A. Wittinghofer, H.R. Kalbitzer, Conformational transitions in p21 ras and in its complexes with the effector protein Raf-RBD and the GTPase activating protein GAP, Biochemistry 35 (1996) 10308-10320.

[26] M. Spoerner, C. Herrmann, I.R. Vetter, H.R. Kalbitzer, A. Wittinghofer, Dynamic properties of the Ras switch I region and its importance for binding to effectors, Proceedings of the National Academy of Sciences 98 (2001) 4944-4949.

[27] J. Liao, F. Shima, M. Araki, M. Ye, S. Muraoka, T. Sugimoto, M. Kawamura, N. Yamamoto, A. Tamura, T. Kataoka, Two conformational states of Ras GTPase exhibit differential GTP-binding kinetics, Biochemical and biophysical research communications 369 (2008) 327-332.

[28] M. Spoerner, A. Wittinghofer, H.R. Kalbitzer, Perturbation of the conformational equilibria in Ras by selective mutations as studied by P 31 NMR spectroscopy, FEBS letters 578 (2004) 305-310.

[29] M. Spoerner, C. Hozsa, J.A. Poetzl, K. Reiss, P. Ganser, M. Geyer, H.R. Kalbitzer, Conformational states of human rat sarcoma (Ras) protein complexed with its natural ligand GTP and their role for effector interaction and GTP hydrolysis, Journal of Biological Chemistry 285 (2010) 39768-39778.

[30] M. Spoerner, A. Nuehs, P. Ganser, C. Herrmann, A. Wittinghofer, H.R. Kalbitzer, Conformational states of Ras complexed with the GTP analogue GppNHp or GppCH2p: implications for the interaction with effector proteins, Biochemistry 44 (2005) 2225-2236.

[31] K.A. Wong, A. Russo, X. Wang, Y.-J. Chen, A. Lavie, J.P. O'Bryan, A New Dimension to Ras Function: A Novel Role for Nucleotide-Free Ras in Class II Phosphatidylinositol 3-Kinase Beta (PI3KC2β) Regulation, PLOS ONE 7 (2012) e45360.

[32] B. Zhang, Y. Zhang, E. Shacter, Y. Zheng, Mechanism of the guanine nucleotide exchange reaction of Ras GTPase evidence for a GTP/GDP displacement model, Biochemistry 44 (2005) 2566-2576.

[33] K. Koera, K. Nakamura, K. Nakao, J. Miyoshi, K. Toyoshima, T. Hatta, H. Otani, A. Aiba, M. Katsuki, K-ras is essential for the development of the mouse embryo, Oncogene 15 (1997) 1151.

[34] L.M. Esteban, C. Vicario-Abejón, P. Fernández-Salguero, A. Fernández-Medarde, N. Swaminathan, K. Yienger, E. Lopez, M. Malumbres, R. McKay, J.M. Ward, Targeted

genomic disruption of H-ras and N-ras, individually or in combination, reveals the dispensability of both loci for mouse growth and development, Molecular and cellular biology 21 (2001) 1444-1452.

[35] J.-A. Choi, M.-T. Park, C.-M. Kang, H.-D. Um, S. Bae, K.-H. Lee, T.-H. Kim, J.-H. Kim, C.-K. Cho, Y.-S. Lee, Opposite effects of Ha-Ras and Ki-Ras on radiation-induced apoptosis via differential activation of PI3K/Akt and Rac/p38 mitogen-activated protein kinase signaling pathways, Oncogene 23 (2004) 9-20.

[36] A.B. Walsh, D. Bar-Sagi, Differential activation of the Rac pathway by Ha-Ras and K-Ras, Science signaling 276 (2001) 15609.

[37] J. Yan, S. Roy, A. Apolloni, A. Lane, J.F. Hancock, Ras isoforms vary in their ability to activate Raf-1 and phosphoinositide 3-kinase, Journal of Biological Chemistry 273 (1998) 24052-24056.

[38] M.D. Vos, C.A. Ellis, C. Elam, A.S. Ülkü, B.J. Taylor, G.J. Clark, RASSF2 is a novel K-Ras-specific effector and potential tumor suppressor, Journal of Biological Chemistry 278 (2003) 28045-28051.

[39] G. Kumari, P.K. Singhal, M. Rao, S. Mahalingam, Nuclear transport of Ras-associated tumor suppressor proteins: different transport receptor binding specificities for arginine-rich nuclear targeting signals, Journal of molecular biology 367 (2007) 1294-1311.

[40] P. Villalonga, C. López-Alcalá, M. Bosch, A. Chiloeches, N. Rocamora, J. Gil, R. Marais, C.J. Marshall, O. Bachs, N. Agell, Calmodulin binds to K-Ras, but not to H- or N-Ras, and modulates its downstream signaling, Molecular and cellular biology 21 (2001) 7345-7354.

[41] S. Roy, R. Luetterforst, A. Harding, A. Apolloni, M. Etheridge, E. Stang, B. Rolls, J.F. Hancock, R.G. Parton, Dominant-negative caveolin inhibits H-Ras function by disrupting cholesterol-rich plasma membrane domains, Nature Cell Biology 1 (1999) 98-105.

[42] S.J. Plowman, N. Ariotti, A. Goodall, R.G. Parton, J.F. Hancock, Electrostatic interactions positively regulate K-Ras nanocluster formation and function, Molecular and cellular biology 28 (2008) 4377-4385.

[43] I.A. Prior, C. Muncke, R.G. Parton, J.F. Hancock, Direct visualization of Ras proteins in spatially distinct cell surface microdomains, Science signaling 160 (2003) 165.

[44] G. Elad-Sfadia, R. Haklai, E. Balan, Y. Kloog, Galectin-3 augments K-Ras activation and triggers a Ras signal that attenuates ERK but not phosphoinositide 3-kinase activity, Journal of Biological Chemistry 279 (2004) 34922-34930.

[45] E. Castellano, E. Santos, Functional Specificity of Ras Isoforms So Similar but So Different, Genes & cancer 2 (2011) 216-231.

[46] C. Herrmann, G.A. Martin, A. Wittinghofer, Quantitative analysis of the complex between p21 and the Ras-binding domain of the human Raf-1 protein kinase, Journal of Biological Chemistry 270 (1995) 2901-2905.

[47] P. Rodriguez-Viciana, P.H. Warne, A. Khwaja, B.M. Marte, D. Pappin, P. Das, M.D. Waterfield, A. Ridley, J. Downward, Role of phosphoinositide 3-OH kinase in cell transformation and control of the actin cytoskeleton by Ras, Cell 89 (1997) 457-467.

[48] M.K. Jones, J.H. Jackson, Ras-GRF activates Ha-Ras, but Not N-Ras or K-Ras 4B, proteinin vivo, Journal of Biological Chemistry 273 (1998) 1782-1787.

[49] H. Kiaris, D.A. Spandidos, Mutations of ras genes in human tumours (Review), International journal of oncology 7 (1995) 413-421.

[50] I.A. Prior, P.D. Lewis, C. Mattos, A comprehensive survey of Ras mutations in cancer, Cancer research 72 (2012) 2457-2467.

[51] S. Eser, N. Reiff, M. Messer, B. Seidler, K. Gottschalk, M. Dobler, M. Hieber, A. Arbeiter, S. Klein, B. Kong, Selective Requirement of PI3K/PDK1 Signaling for Kras Oncogene-Driven Pancreatic Cell Plasticity and Cancer, Cancer Cell (2013).

[52] H. Huang, J. Daniluk, Y. Liu, J. Chu, Z. Li, B. Ji, C. Logsdon, Oncogenic K-Ras requires activation for enhanced activity, Oncogene (2013).

[53] S. Schubbert, K. Shannon, G. Bollag, Hyperactive Ras in developmental disorders and cancer, Nature Reviews Cancer 7 (2007) 295-308.

[54] M. Bentires-Alj, M.I. Kontaridis, B.G. Neel, Stops along the RAS pathway in human genetic disease, Nature medicine 12 (2006) 283-286.

[55] Y. Aoki, T. Niihori, H. Kawame, K. Kurosawa, H. Ohashi, Y. Tanaka, M. Filocamo, K. Kato, Y. Suzuki, S. Kure, Germline mutations in HRAS proto-oncogene cause Costello syndrome, Nature genetics 37 (2005) 1038.

[56] D.A. Tuveson, A.T. Shaw, N.A. Willis, D.P. Silver, E.L. Jackson, S. Chang, K.L. Mercer, R. Grochow, H. Hock, D. Crowley, Endogenous oncogenic< i> K-rasG12D</i> stimulates proliferation and widespread neoplastic and developmental defects, Cancer cell 5 (2004) 375-387.

[57] D. Bucher, B.J. Grant, J.A. McCammon, Induced fit or conformational selection? The role of the semi-closed state in the maltose binding protein, Biochemistry 50 (2011) 10530-10539.

[58] M. Trellet, A.S. Melquiond, A.M. Bonvin, A Unified Conformational Selection and Induced Fit Approach to Protein-Peptide Docking, PLOS ONE 8 (2013) e58769.

[59] B.J. Grant, A.A. Gorfe, J.A. McCammon, Ras conformational switching: simulating nucleotide-dependent conformational transitions with accelerated molecular dynamics, PLoS computational biology 5 (2009) e1000325.

[60] C. Kiel, D. Filchtinski, M. Spoerner, G. Schreiber, H.R. Kalbitzer, C. Herrmann, Improved Binding of Raf to Ras· GDP Is Correlated with Biological Activity, Journal of Biological Chemistry 284 (2009) 31893-31902.

[61] N. Nassar, G. Horn, C.A. Herrmann, A. Scherer, F. McCormick, A. Wittinghofer, The 2.2 Å crystal structure of the Ras-binding domain of the serine/threonine kinase c-Raf1 in complex with RaplA and a GTP analogue, Nature 375 (1995) 554-560.

[62] J.A. McCammon, S.C. Harvey, Dynamics of proteins and nucleic acids, Cambridge University Press, 1988.

[63] D. Frenkel, B. Smit, M.A. Ratner, Understanding molecular simulation: from algorithms to applications, Physics Today 50 (1997) 66.

[64] D.W. Borhani, D.E. Shaw, The future of molecular dynamics simulations in drug discovery, Journal of computer-aided molecular design 26 (2012) 15-26.

[65] M. Allen, D. Tildesley, Computer simulation of liquids. 1987, New York: Oxford 385.

[66] J.L. Klepeis, K. Lindorff-Larsen, R.O. Dror, D.E. Shaw, Long-timescale molecular dynamics simulations of protein structure and function, Current opinion in structural biology 19 (2009) 120-127.

[67] M. Bhandarkar, R. Brunner, C. Chipot, A. Dalke, S. Dixit, P. Grayson, J. Gullingsrud, A. Gursoy, D. Hardy, W. Humphrey, NAMD User's Guide, Urbana 51 (2003) 61801.

[68] D.I.J.M. Schweifer, A Distributed Computing Environment for Material Sciences, Citeseer, 2006.

[69] W. Humphrey, A. Dalke, K. Schulten, VMD: visual molecular dynamics, Journal of molecular graphics 14 (1996) 33-38.

[70] B.J. Grant, A.P.C. Rodrigues, K.M. ElSawy, J.A. McCammon, L.S.D. Caves, Bio3d: an R package for the comparative analysis of protein structures, Bioinformatics 22 (2006) 2695-2696.

[71] M. Seeber, M. Cecchini, F. Rao, G. Settanni, A. Caflisch, Wordom: a program for efficient analysis of molecular dynamics simulations, Bioinformatics 23 (2007) 2625-2627.

[72] W. Kabsch, Automatic processing of rotation diffraction data from crystals of initially unknown symmetry and cell constants, Journal of applied crystallography 26 (1993) 795-800.

[73] T. Ichiye, M. Karplus, Collective motions in proteins: a covariance analysis of atomic fluctuations in molecular dynamics and normal mode simulations, Proteins: Structure, Function, and Bioinformatics 11 (1991) 205-217.

[74] A. Altis, P.H. Nguyen, R. Hegger, G. Stock, Dihedral angle principal component analysis of molecular dynamics simulations, The Journal of chemical physics 126 (2007) 244111.

[75] J.M. Berg, J.L. Tymoczko, L. Stryer, Chemical Bonds in Biochemistry, (2002).

[76] T.L. Brown, H.E. LeMay, R. Wilson, Chemistry: The central science, Prentice Hall Englewood Cliffs, NJ, 1988.

[77] S. Kumar, H. Wolfson, R. Nussinov, Protein flexibility and electrostatic interactions, IBM Journal of Research and Development 45 (2001) 499-512.

[78] A.S. Thomas, A.H. Elcock, Molecular simulations suggest protein salt bridges are uniquely suited to life at high temperatures, Journal of the American Chemical Society 126 (2004) 2208-2214.

[79] K. Takano, K. Tsuchimori, Y. Yamagata, K. Yutani, Contribution of salt bridges near the surface of a protein to the conformational stability, Biochemistry 39 (2000) 12375-12381.

[80] R.O. Dror, D.H. Arlow, D.W. Borhani, M.Ø. Jensen, S. Piana, D.E. Shaw, Identification of two distinct inactive conformations of the β2-adrenergic receptor reconciles structural and biochemical observations, Proceedings of the National Academy of Sciences 106 (2009) 4689-4694.

[81] S.H. Lee, J.W. Lee, Y.H. Soung, H.S. Kim, W.S. Park, S.Y. Kim, J.H. Lee, J.Y. Park, Y.G. Cho, C.J. Kim, BRAF and KRAS mutations in stomach cancer, Oncogene 22 (2003) 6942-6945.

[82] L. Gremer, T. Merbitz-Zahradnik, R. Dvorsky, I.C. Cirstea, C.P. Kratz, M. Zenker, A. Wittinghofer, M.R. Ahmadian, Germline KRAS mutations cause aberrant biochemical and physical properties leading to developmental disorders, Human mutation 32 (2011) 33-43.

[83] J. John, I. Schlichting, E. Schiltz, P. Rösch, A. Wittinghofer, C-terminal truncation of p21H preserves crucial kinetic and structural properties, Journal of Biological Chemistry 264 (1989) 13086-13092.

[84] M.A. White, C. Nicolette, A. Minden, A. Polverino, L.V. Aelst, M. Karin, M.H. Wigler, Multiple Ras functions can contribute to mammalian cell transformation, Cell 80 (1995) 533-542.

[85] F.C. Bernstein, T.F. Koetzle, G.J. Williams, E.F. Meyer, M.D. Brice, J.R. Rodgers, O. Kennard, T. Shimanouchi, M. Tasumi, The protein data bank: a computer-based archival file for macromolecular structures, Archives of biochemistry and biophysics 185 (1978) 584-591.

[86] J.C. Phillips, R. Braun, W. Wang, J. Gumbart, E. Tajkhorshid, E. Villa, C. Chipot, R.D. Skeel, L. Kale, K. Schulten, Scalable molecular dynamics with NAMD, Journal of computational chemistry 26 (2005) 1781-1802.

[87] A.D. MacKerell Jr, D. Bashford, M. Bellott, R.L. Dunbrack Jr, J. Evanseck, M. Field, S. Fischer, J.a. Gao, H. Guo, S.a. Ha, All-atom empirical potential for molecular modeling and dynamics studies of proteins, The Journal of Physical Chemistry B 102 (1998) 3586-3616.

[88] J.-P. Ryckaert, G. Ciccotti, H.J. Berendsen, Numerical integration of the cartesian equations of motion of a system with constraints: molecular dynamics of< i> n</i>-alkanes, Journal of Computational Physics 23 (1977) 327-341.

[89] T. Darden, D. York, L. Pedersen, Particle mesh Ewald: An N· log (N) method for Ewald sums in large systems, The Journal of chemical physics 98 (1993) 10089.

[90] S.A. Adcock, J.A. McCammon, Molecular dynamics: survey of methods for simulating the activity of proteins, Chemical reviews 106 (2006) 1589.

[91] J. McCammon, Protein dynamics, Reports on Progress in Physics 47 (1984) 1.

[92] R. Team, R: A Language and Environment for Statistical Computing. R Foundation for Statistical Computing, Vienna, Austria, 2007, ISBN 3-900051-07-0, 2010.

[93] P.W. Howe, Principal components analysis of protein structure ensembles calculated using NMR data, Journal of biomolecular NMR 20 (2001) 61-70.

[94] A.A. Gorfe, B.J. Grant, J.A. McCammon, Mapping the nucleotide and isoform-dependent structural and dynamical features of Ras proteins, Structure 16 (2008) 885-896.

[95] M.V. Milburn, L. Tong, A.M. DeVos, A. Brünger, Z. Yamaizumi, S. Nishimura, S.-H. Kim, Molecular switch for signal transduction: structural differences between active and inactive forms of protooncogenic ras proteins, Science 247 (1990) 939-945.

[96] L. Tong, A.M. de Vos, M.V. Milburn, S.-H. Kim, Crystal structures at 2.2 A resolution of the catalytic domains of normal ras protein and an oncogenic mutant complexed with GDP, Journal of molecular biology 217 (1991) 503.

[97] E. Mooi, M. Sarstedt, A concise guide to market research: The process, data, and methods using IBM SPSS statistics, Springer, 2011.

[98] F. Shima, Y. Ijiri, S. Muraoka, J. Liao, M. Ye, M. Araki, K. Matsumoto, N. Yamamoto, T. Sugimoto, Y. Yoshikawa, Structural basis for conformational dynamics of GTP-bound Ras protein, Journal of Biological Chemistry 285 (2010) 22696-22705.

[99] S. Wohlgemuth, C. Kiel, A. Kramer, L. Serrano, F. Wittinghofer, C. Herrmann, Recognizing and defining true Ras binding domains I: biochemical analysis, Journal of molecular biology 348 (2005) 741-758.

[100] D.D. Boehr, R. Nussinov, P.E. Wright, The role of dynamic conformational ensembles in biomolecular recognition, Nature chemical biology 5 (2009) 789-796.

[101] B. Antonny, P. Chardin, M. Roux, M. Chabre, GTP hydrolysis mechanisms in ras p21 and in the ras-GAP complex studied by fluorescence measurements on tryptophan mutants, Biochemistry 30 (1991) 8287-8295.

[102] M.J. Smith, B.G. Neel, M. Ikura, NMR-based functional profiling of RASopathies and oncogenic RAS mutations, Proceedings of the National Academy of Sciences (2013).

[103] S.A. Moodie, M. Paris, E. Villafranca, P. Kirshmeier, B.M. Willumsen, A. Wolfman, Different structural requirements within the switch II region of the Ras protein for interactions with specific downstream targets, Oncogene 11 (1995) 447.

[104] W. Li, M. Melnick, N. Perrimon, Dual function of Ras in Raf activation, Development 125 (1998) 4999-5008.

[105] J.K. Drugan, R. Khosravi-Far, M.A. White, C.J. Der, Y.J. Sung, Y.W. Hwang, S.L. Campbell, Ras Interaction with Two Distinct Binding Domains in Raf-1 5 Be Required for Ras Transformation, Journal of Biological Chemistry 271 (1996) 233-237.

[106] C. Lopez-Alcalá, B. Alvarez-Moya, P. Villalonga, M. Calvo, O. Bachs, N. Agell, Identification of essential interacting elements in K-Ras/calmodulin binding and its role in K-Ras localization, Journal of Biological Chemistry 283 (2008) 10621-10631.

[107] B. Stieglitz, C. Bee, D. Schwarz, Ö. Yildiz, A. Moshnikova, A. Khokhlatchev, C. Herrmann, Novel type of Ras effector interaction established between tumour suppressor NORE1A and Ras switch II, The EMBO journal 27 (2008) 1995-2005.

[108] H. Gohlke, L.A. Kuhn, D.A. Case, Change in protein flexibility upon complex formation: Analysis of Ras-Raf using molecular dynamics and a molecular

framework approach, Proteins: Structure, Function, and Bioinformatics 56 (2004) 322-337.

[109] M.J. Betts, R.B. Russell, Amino acid properties and consequences of substitutions, Bioinformatics for geneticists 317 (2003) 289.

[110] P. Rodriguez-Viciana, C. Sabatier, F. McCormick, Signaling specificity by Ras family GTPases is determined by the full spectrum of effectors they regulate, Molecular and cellular biology 24 (2004) 4943-4954.

[111] J.C. Lacal, F.P. McCormick, The ras superfamily of GTPases, CRC PressI Llc, 1993.

[112] A.T. Sasaki, A. Carracedo, J.W. Locasale, D. Anastasiou, K. Takeuchi, E.R. Kahoud, S. Haviv, J.M. Asara, P.P. Pandolfi, L.C. Cantley, Ubiquitination of K-Ras enhances activation and facilitates binding to select downstream effectors, Science signaling 4 (2011) ra13.

[113] J.H. Peters, B.L. de Groot, Ubiquitin Dynamics in Complexes Reveal Molecular Recognition Mechanisms Beyond Induced Fit and Conformational Selection, PLoS Computational Biology 8 (2012) e1002704.

[114] M.-C.C. Hwang, Y.-J. Sung, Y.-W. Hwang, The differential effects of the Gly-60 to Ala mutation on the interaction of H-Ras p21 with different downstream targets, Journal of Biological Chemistry 271 (1996) 8196-8202.

[115] A.A. Gorfe, M. Hanzal-Bayer, D. Abankwa, J.F. Hancock, J.A. McCammon, Structure and dynamics of the full-length lipid-modified H-Ras protein in a 1, 2-dimyristoylglycero-3-phosphocholine bilayer, Journal of medicinal chemistry 50 (2007) 674-684.

[116] D. Abankwa, A.A. Gorfe, K. Inder, J.F. Hancock, Ras membrane orientation and nanodomain localization generate isoform diversity, Proceedings of the National Academy of Sciences 107 (2010) 1130-1135.

[117] B.R. Miller III, T.D. McGee Jr, J.M. Swails, N. Homeyer, H. Gohlke, A.E. Roitberg, MMPBSA. py: An Efficient Program for End-State Free Energy Calculations, Journal of Chemical Theory and Computation 8 (2012) 3314-3321.

[118] D. Bucher, B.J. Grant, P.R. Markwick, J.A. McCammon, Accessing a hidden conformation of the maltose binding protein using accelerated molecular dynamics, PLoS computational biology 7 (2011) e1002034.

[119] T. Miyata, Y. Ikuta, F. Hirata, Thermodynamic Integration Based on Molecular Dynamics Simulation Combined with 3D-RISM Theory,  (2009).

# VITA

Nandini Rambahal was born in Trinidad and Tobago. She moved to Florida when she was 16 where she completed high school. She obtained first her A.A degree in Pre Medical Studies from Broward College and then went on to obtain B.S. degrees in both Chemistry and Molecular Biology from Florida Atlantic University. She joined GSBS in 2009 and after a year of teaching Chemistry and another year working with Dr. Qingchun Tong, joined the Gofe group in May 2011. Oddly enough she does have a strange obsession with dancing even the ones that proteins do.